

---

# DOMAIN DECOMPOSITION METHODS AND PRECONDITIONING STRATEGIES USING GENERALIZED LOCALLY TOEPLITZ TOOLS: PROPOSALS, ANALYSIS, AND NUMERICAL VALIDATION

---

A. Rifqui

abdessadek.rifqui@um6p.ma

A. Ratnani

ahmed.ratnani@um6p.ma

S. Serra-Capizzano

s.serracapizzano@uninsubria.it

February 5, 2026

## ABSTRACT

In the current work we present a spectral analysis of the additive and multiplicative Schwarz methods within the framework of domain decomposition techniques, by investigating the spectral properties of these classical Schwarz preconditioning matrix-sequences, with emphasis on their convergence behavior and on the effect of transmission operators. In particular, after a general presentation of various options, we focus on restricted variants of the Schwarz methods aimed at improving parallel efficiency, while preserving their convergence features. In order to rigorously describe and analyze the convergence behavior, we employ the theory of generalized locally Toeplitz (GLT) sequences, which provides a robust framework for studying the asymptotic spectral distribution of the discretized operators arising from Schwarz iterations. By associating each operator sequence with the appropriate GLT symbol, we derive explicit expressions for the GLT symbols of the convergence factors, for both additive and multiplicative Schwarz methods. The GLT-based spectral approach offers a unified and systematic understanding of how the spectrum evolves with mesh refinement and overlap size (in the algebraic case). Our analysis not only deepens the theoretical understanding of classical Schwarz methods, but also establishes a foundation for examining future restricted or hybrid Schwarz variants using symbolic spectral tools. These results enable the prediction of the remarkable efficiency of block Jacobi/Gauss–Seidel and block additive/multiplicative Schwarz preconditioners for GLT sequences, as further illustrated through a wide choice of numerical experiments.

**Keywords:** Isogeometric analysis, domain decomposition, Krylov methods, spectral and singular value distribution, generalized locally Toeplitz (GLT) sequences, GLT symbol, block Jacobi and Gauss–Seidel, block additive, block multiplicative, block restricted additive, block restricted multiplicative, Schwarz methods.

## 1 Introduction

Basic Finite Difference and Finite Element discretizations of partial differential equations (PDEs) in  $d$ -dimensional domains,  $d \geq 1$ , typically lead to  $d$ -level banded matrices, such as  $d$ -level tridiagonal or  $d$ -level pentadiagonal systems. In Isogeometric Analysis (IgA) [41], these structures remain of  $d$ -level type, but they become of larger bandwidth due to the higher continuity of spline bases, resulting in large, highly structured, and spectrally rich matrices. As the spline degree  $p$  increases ( $p$ -refinement), the system matrices gain more nonzero entries per row at any of the  $d$  levels, significantly increasing computational cost. This makes the design of robust and scalable solvers for high-degree spline discretizations both challenging and essential, motivating ongoing research in efficient iterative methods [22, 19, 48, 21, 40]. Similar remarks apply to Finite Elements of higher degree, where the bandwidth remains fixed but the scalar entries are replaced by blocks of fixed size depending on the degree and on  $d$ : hence we have again an increase of the structural complexity for solving the associated linear systems [35, 47].

Schwarz methods play a fundamental role in solving PDEs numerically. They decompose the computational domain into subdomains and solve local problems exactly or approximately within each subdomain. In the classical Schwarz

formulation, Dirichlet conditions are imposed on the artificial interfaces between subdomains [44, 53, 55, 46]. Algebraic interpretations of classical Schwarz methods have been instrumental in understanding their structure and guiding extensions [54, 38, 26, 14]. In particular, additive and multiplicative Schwarz methods, as well as their corresponding preconditioners, are algebraically equivalent to block Jacobi and block Gauss–Seidel methods, respectively, with the addition of subdomain overlap.

However, the convergence analysis of the related iterative solvers show difficulties. Often the matrix-size is large, but, more interestingly, the request of robustness of the methods with respect to problem and discretization parameters implies that the convergence analysis should be done parametrically, i.e. at least with respect to the fineness parameter  $h = h_n$  (or parameters in the  $d$  level setting), the latter tending to zero as we require more and more accurate solutions. From a matrix-theoretic perspective, the fact that  $h = h_n$  tends to zero corresponds to the fact that the matrix-size  $d_n$  tends to infinity. In other words, the analysis can be framed naturally from the point of view of asymptotic linear algebra [18, 10], and in fact we are not interested to the single matrix  $A_n$ , but to the whole sequence of matrices  $\{A_n\}_n$  with  $A_n$  of size  $d_n \times d_n$ ,  $d_n \rightarrow \infty$  as  $n \rightarrow \infty$ .

When considering the discretization of a PDE with constant coefficients, uniform meshing, on a Cartesian domain, Dirichlet boundary conditions, we end up with  $d$ -level Toeplitz structures, sometimes also of block type when considering Finite Elements of high order, Isogeometric Analysis of intermediate regularity, Discontinuous Galerkin; see [8, 9] and references therein. However, this represents a special case and the violation of any of the conditions listed above spoils the Toeplitzness of the underlying coefficient matrices. In particular, while the change in the boundary conditions can be seen as an asymptotically low-rank correction of the Toeplitz structure, the other changes leads to matrix-sequences of non Toeplitz global structure, but still with hidden local Toeplitzness. The theory of generalized locally Toeplitz (GLT) sequences provides a unified framework for analyzing spectral and singular value distributions of matrix-sequences with a (possibly hidden) Toeplitz-like structure, as arising in the approximation of PDEs under general conditions; see [6, 8, 9, 30, 31] for the general theory and [29, 32, 33] for application oriented surveys. Such sequences naturally arise in the discretization of differential and integral equations [51, 30, 31], and their study has led to deep connections with function spaces, spectral approximation, and operator theory [10]. The spectral and singular value distributions of a GLT sequence plays a central role in: (i) assessing the spectral accuracy of discretizations [16], (ii) verifying preservation of the average spectral gap [15], and (iii) predicting eigenvalue distributions analytically [31]. Moreover, GLT-based analysis enables precise convergence estimates for iterative solvers such as Krylov methods [51, 30, 31]. More importantly, the GLT allows to suggest analyze ad hoc innovative preconditioning strategies, multigrid operators, and multi-iterative methods. In this direction a clear example is given by the design of multigrid and multi-iterative solvers for high degree Isogeometric analysis in which the preconditioned Krylov preconditioning is directly suggested by the GLT analysis [22]; see also [40] for a complementary approach based on the study of ad hoc approximation spaces.

## Main Contributions

Under the assumption that  $\{A_n\}$  is a matrix-sequence arising from the discretization of an elliptic problem or, more generally, that  $\{A_n\}$  may denote any block-structured matrix-sequence admitting a GLT symbol  $\kappa(\mathbf{x}, \boldsymbol{\theta})$ , we give the following contributions.

- Within the GLT framework and from a purely algebraic viewpoint, when there is no overlap we prove that both the additive Schwarz operator and the multiplicative Schwarz operator generate matrix-sequences  $\{P_n\}$  such that

$$\{P_n\} \sim_{\text{GLT}} \kappa(\mathbf{x}, \boldsymbol{\theta}).$$

In the overlapping case, the multiplicative Schwarz operator and its restricted variants show the same property, while this is not true for the additive Schwarz operator: in the latter case, restriction is necessary for guaranteeing the relation  $\{P_n\} \sim_{\text{GLT}} \kappa(\mathbf{x}, \boldsymbol{\theta})$ .

- In agreement with the previous item, except for the case of additive Schwarz with overlapping, we show that the preconditioned matrix-sequences associated with all the previous methods satisfy

$$\{P_n^{-1} A_n\} \sim_{\text{GLT}} 1,$$

thereby providing a rigorous spectral-distribution justification for the use of the related preconditioned methods.

- The GLT analysis provides also constructive suggestions on new variants of the previous techniques showing the same key property  $\{P_n^{-1} A_n\} \sim_{\text{GLT}} 1$  for the preconditioned matrix-sequences.

Of course, outliers can be present and they can drastically deteriorate the performances of  $P_n$  as preconditioner, especially if they approach the zero. We take care of this case as well, by proving few computationally affordable strategies: in this direction we mention that this work starts to answer to new research lines indicated in [34].

### Organization of the Work

In Section 2 we introduce block preconditioners which are used in the context of domain decomposition techniques. Section 3 is devoted to introduce the axioms that characterize the GLT theory and other tools recently developed for block structures.

In Section 4, we analyze a family of Schwarz block preconditioners within the GLT framework. Leveraging a preliminary result on the positivity of matrix-valued GLT symbols.

Section 5 presents our main results: a unified GLT-based analysis of Schwarz block preconditioners for Toeplitz and general GLT sequences. We prove that block Jacobi, block Gauss–Seidel, additive, restricted, and multiplicative Schwarz preconditioners all preserve the GLT symbol of the underlying sequence. As a consequence, the preconditioned matrices exhibit spectral clustering at 1, ensuring rapid convergence of Krylov methods. These results provide the first comprehensive GLT-theoretic justification for the effectiveness of Schwarz-type preconditioners.

In Section 6, we present numerical experiments that validate our theoretical predictions, showing that the proposed Schwarz operators perform effectively both as standalone iterative methods and as preconditioners within Krylov solvers. Finally, Section 7 concludes the paper and discusses future research directions.

## 2 Iterative methods with classical block preconditioners

The main objective of this study is to design and analyze an optimal solver based on the domain decomposition method for the linear system

$$A_n u = F, \quad (1)$$

where  $A_n$  is a square matrix of size  $d_n \times d_n$ .

In general, the global matrix  $A_n$  exhibits a block-tridiagonal structure associated with a decomposition of the computational domain  $\Omega$  into  $\nu$  overlapping or non-overlapping subdomains  $\Omega_1, \dots, \Omega_\nu$ ,  $\Omega = \cup_{i=1}^\nu \Omega_i$ . In the context of the present work we consider mainly  $\Omega = [0, 1]$ ,  $\Omega_i = [a_i, b_i]$ ,  $a_i < b_i$ ,  $i = 1, \dots, \nu$ .

The latter decomposition leads to a block-structured linear system of the form

$$A_n = \begin{bmatrix} A_{11} & A_{12} & O & \cdots & O \\ A_{21} & A_{22} & A_{23} & \ddots & \vdots \\ O & A_{32} & A_{33} & \ddots & O \\ \vdots & \ddots & \ddots & \ddots & A_{3(\nu-1),3\nu-2} \\ O & \cdots & O & A_{3\nu-2,3(\nu-1)} & A_{3\nu-2,3\nu-2} \end{bmatrix}, \quad (2)$$

where each block  $A_{ij}$  is of dimension  $n_i \times n_j$ , and the total size satisfies

$$d_n = \sum_{i=1}^{3\nu-2} n_i.$$

The diagonal blocks  $A_{ii}$  correspond to the discrete operators on each subdomain  $\Omega_i$ , while the off-diagonal blocks  $A_{i,i+1}$  and  $A_{i+1,i}$  encode the coupling between neighboring overlapping or non-overlapping subdomains.

**Particular case:  $\nu = 2$ .** For a decomposition into two overlapping subdomains, the global matrix exhibits a four-block structure:

$$A_n = \begin{bmatrix} A_{11} & A_{12} & O & O \\ A_{21} & A_{22} & A_{23} & O \\ O & A_{32} & A_{33} & A_{34} \\ O & O & A_{43} & A_{44} \end{bmatrix}, \quad (3)$$

where each block  $A_{ij}$  has dimension  $d_{n_i} \times d_{n_j}$  for  $i, j = 1, \dots, 4$ , and  $d_n = \sum_{i=1}^4 n_i = \sum_{i=1}^2 d_i(n)$ ,  $d_1(n) = n_1 + n_2$ ,  $d_2(n) = n_3 + n_4$ . This structure is typically unbalanced, with

$$n_1 \gg n_2 \quad \text{and} \quad n_4 \gg n_3,$$

reflecting large interior subdomains and comparatively small overlapping regions. The considered configuration is the one schematically illustrated in Figure 1, which shows the sparsity pattern of the global matrix for the two-subdomain overlapping decomposition.

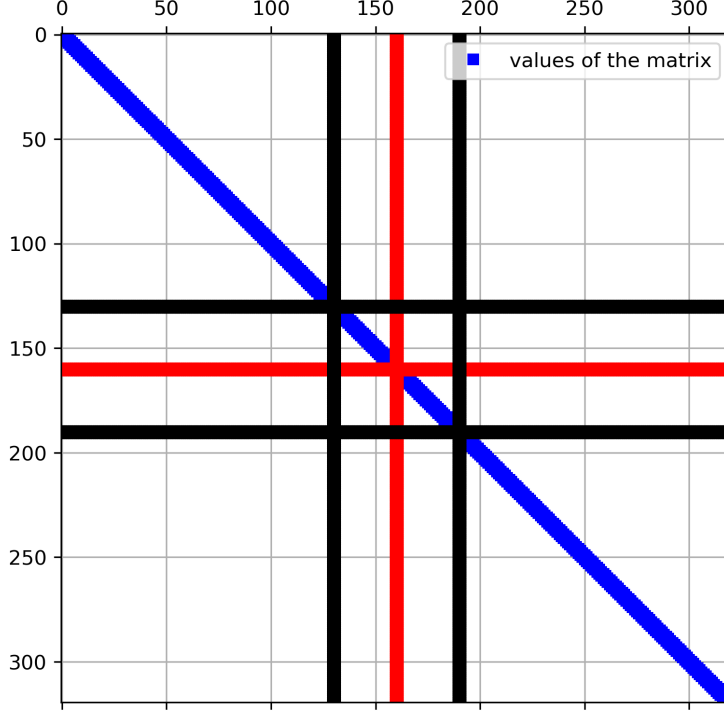


Figure 1: A  $320 \times 320$  band matrix partitioned into  $4 \times 4$  blocks, with block sizes  $n_1 = n_4 = 130$  and  $n_2 = n_3 = 30$ .

- We first consider the following **diagonal block** (without overlap):

$$\text{BlockDiag}_{d_1(n), d_2(n)}(A_n) = \begin{bmatrix} A_1 & O \\ O & A_2 \end{bmatrix}, \quad (4)$$

where each block  $A_i$  is given by

$$A_1 = \begin{bmatrix} A_{11} & A_{12} \\ A_{21} & A_{22} \end{bmatrix}, \quad \text{and} \quad A_2 = \begin{bmatrix} A_{33} & A_{34} \\ A_{43} & A_{44} \end{bmatrix}, \quad (5)$$

which are square but not necessarily of the same size. The operators  $\text{BlockDiag}(\cdot)$  are studied in some detail in [34] in connection with the new class of generalized locally Hankel matrix-sequences.

The corresponding **block Jacobi preconditioner**  $P_n$  is that defined in (4) and we have

$$P_n^{-1} = \left( P_{BJ,n}^{(\nu=2)}(A_n) \right)^{-1} := \left( \text{BlockDiag}_{d_1(n), d_2(n)}(A_n) \right)^{-1} = \begin{bmatrix} A_1^{-1} & O \\ O & A_2^{-1} \end{bmatrix} = \sum_{j=1}^{\nu=2} R_j^T A_j^{-1} R_j, \quad (6)$$

where the restriction operators are defined as

$$R_1 = [I_{d_1(n)} \quad O], \quad R_2 = [O \quad I_{d_2(n)}], \quad (7)$$

of respective dimensions  $(n_1 + n_2) \times d_n$  and  $(n_3 + n_4) \times d_n$ ,  $d_1(n) = n_1 + n_2$ ,  $d_2(n) = n_3 + n_4$ . For each  $i = 1, \dots, \nu$ , the transposes  $R_i^T$  act as **prolongation operators**. The terminology is standard in the multigrid literature.

The standard **block Jacobi iteration** using these two blocks ( $\nu = 2$ ) has the iteration operator

$$T_n = T_{BJ,n}^{(\nu=2)}(A_n) := I - \left( P_{BJ,n}^{(\nu=2)} \right)^{-1} A_n. \quad (8)$$

For a given initial vector  $u_0$ , the iterative scheme is expressed as

$$u^{k+1} = T_n u^k + P_n^{-1} F, \quad k = 0, 1, 2, \dots,$$

and converges linearly with an asymptotic convergence factor  $\rho(T_n)$ , the spectral radius of the iteration operator. Later, we will analyze the spectral features of the matrix-sequence  $\{T_n\}$  in detail, using the GLT theory.

- Similarly, using the  $\text{BlockTril}(\cdot)$  operators studied in [34], the **block Gauss-Seidel preconditioner** (without overlap) is defined as

$$\begin{aligned} P_n^{-1} &= \left( P_{BGS,n}^{(\nu=2)}(A_n) \right)^{-1} := \left( \text{BlockTril}_{d_1(n), d_2(n)}(A_n) \right)^{-1} = \\ &= \begin{bmatrix} A_1 & O \\ A'_1 & A_2 \end{bmatrix}^{-1} = \left( I - \prod_{j=\nu=2}^1 (I - R_j^T A_j^{-1} R_j A_n) \right) A_n^{-1}, \end{aligned}$$

where the coupling block  $A'_1$  is given by

$$A'_1 = \begin{bmatrix} O & A_{32} \\ O & O \end{bmatrix},$$

and the blocks  $A_1, A_2$  as well as the restriction operators  $R_1$  and  $R_2$  are the same as in the previous block Jacobi definition. Again The standard **block Gauss-Seidel iteration** using these two blocks ( $\nu = 2$ ) has the iteration operator

$$T_n = T_{BGS,n}^{(\nu=2)}(A_n) := I - \left( P_{BGS,n}^{(\nu=2)} \right)^{-1} A_n = \prod_{j=\nu=2}^1 (I - R_j^T A_j^{-1} R_j A_n). \quad (9)$$

- Consider now the same blocks (5) with overlap. Using the same notation, the blocks with overlap can be written as

$$A_1 = \begin{bmatrix} A_{11} & A_{12} & O \\ A_{21} & A_{22} & A_{23} \\ O & A_{32} & A_{33} \end{bmatrix}, \quad \text{and} \quad A_2 = \begin{bmatrix} A_{22} & A_{23} & O \\ A_{32} & A_{33} & A_{34} \\ O & A_{43} & A_{44} \end{bmatrix}. \quad (10)$$

The corresponding restriction operators are

$$R_1 = [I_{d_1(n)+n_3} \quad O], \quad R_2 = [O \quad I_{n_2+d_2(n)}], \quad (11)$$

with respective dimensions  $(n_1 + n_2 + n_3) \times d_n$  and  $(n_2 + n_3 + n_4) \times d_n$ .

Using this notation, the **block additive** and **block multiplicative Schwarz preconditioners** are defined as

$$\left( P_{BAS,n}^{(\nu=2)}(A_n) \right)^{-1} := \sum_{j=1}^{\nu=2} R_j^T A_j^{-1} R_j, \quad \left( P_{BMS,n}^{(\nu=2)}(A_n) \right)^{-1} := \left( I - \prod_{j=\nu=2}^1 (I - R_j^T A_j^{-1} R_j A_n) \right) A_n^{-1}, \quad (12)$$

respectively.

**Remark 2.1.** Comparing these blocks, one concludes that the classical Schwarz preconditioners can be regarded as a generalization of **block Jacobi** or **block Gauss-Seidel** preconditioners, with the addition of overlap. In Section 4, when considering the theoretical analysis, we show how to interpret the overlapping case in terms of a combination of several **block Jacobi** or **block Gauss-Seidel** preconditioners, respectively, acting simultaneously: this is the key for using the GLT theoretical machinery in our setting.

- From the explicit expression of the preconditioners (12), one can explicitly write the iteration operators for the additive and multiplicative Schwarz methods as

$$T_{BAS,n}^{(\nu=2)}(A_n) = I - \sum_{i=1}^2 R_i^T A_i^{-1} R_i A_n, \quad (13)$$

$$T_{BMS,n}^{(\nu=2)}(A_n) = \prod_{i=2}^1 (I - R_i^T A_i^{-1} R_i A_n), \quad (14)$$

respectively.

The additive Schwarz iteration (with overlap) associated with the operator  $T_{\text{BAS},n}^{\nu=2}$  is usually **not convergent**, since for overlapping subdomains it holds that  $2I \geq R_i^T R_i \geq I$ , with constants that cannot be improved. To address this, one commonly introduces a relaxation parameter  $0 < \gamma < 1$ . However, an alternative approach is provided by the **restricted additive Schwarz (RAS)** method [25, 20, 27]. In the theoretical section we will show the GLT theory gives an explanation on the reason why one should expect that RAS is fast than the additive Schwarz method with relaxation parameter  $\gamma$ .

The RAS method uses the local solvers with overlap, employing the standard restriction operators  $R_i$ , but uses *prolongation operators without overlap*  $\tilde{R}_i^T$ , defined as

$$\tilde{R}_1 = \begin{bmatrix} I_{d_1(n)} & O \\ O & O \end{bmatrix}, \quad \tilde{R}_2 = \begin{bmatrix} O & O \\ O & I_{d_2(n)} \end{bmatrix}, \quad (15)$$

which have the same dimensions as those of  $R_i$  in (11),  $i = 1, 2$ . Here, the identity in  $\tilde{R}_1$  is of order  $d_1(n) = n_1 + n_2$ , and in  $\tilde{R}_2$  of order  $d_2(n) = n_3 + n_4$ . These operators select only the variables without overlap, so that  $\sum_i \tilde{R}_i^T R_i = I$ , eliminating double counting of variables in the overlap. Under certain assumptions, there is no need for a relaxation parameter to ensure convergence. With this notation, the RAS iteration operator is

$$T_{\text{BRAS},n}^{(\nu=2)}(A_n) = I - \sum_{i=1}^{\nu=2} \tilde{R}_i^T A_i^{-1} R_i A_n. \quad (16)$$

Similarly, the **restricted multiplicative Schwarz (RMS)** [45] iteration operator is defined as

$$T_{\text{BRMS},n}^{(\nu=2)}(A_n) = \prod_{i=\nu=2}^1 \left( I - \tilde{R}_i^T A_i^{-1} R_i A_n \right) = \left( I - \tilde{R}_2^T A_2^{-1} R_2 A_n \right) \left( I - \tilde{R}_1^T A_1^{-1} R_1 A_n \right). \quad (17)$$

**Remark 2.2.** Although for the multiplicative Schwarz the use of  $\tilde{R}_i^T$  is not strictly necessary to avoid double counting. This method is included here for completeness; see Theorem 5.3 for the related analysis.

**Remark 2.3.** By recalling the setting at beginning of Section 2, the general case of  $\nu$  non-overlapping subdomains  $\Omega_1, \dots, \Omega_\nu, [0, 1] = \Omega = \cup_{i=1}^\nu \Omega_i, \Omega_i = [a_i, b_i], a_i < b_i, i = 1, \dots, \nu - 1$ , is described by the conditions  $b_i = a_{i+1}, i = 1, \dots, \nu$ . The general case of  $\nu$  overlapping subdomains is described by the conditions  $a_i < a_{i+1}$  and  $b_i < b_{i+1}, i = 1, \dots, \nu - 1$  - (this ensures that a subdomain is not a subset of another) - and there exists  $j$  such that  $a_{j+1} < b_j$ : the set of the indices  $j \in \{1, \dots, \nu - 1\}$  such that  $a_{j+1} < b_j$  is called  $\mathcal{OV}$ . Furthermore we require  $b_i < a_{i+2}, i = 1, \dots, \nu - 2$ ; otherwise the set  $\Omega_{i+1} \subset \Omega_i \cup \Omega_{i+2}$  would be redundant. When we write that there is overlapping we mean that  $\#\mathcal{OV} \geq 1$ ; conversely,  $\#\mathcal{OV} = 0$  if and only if there is no overlapping.

The latter precise setting allows to describe the general RAS and RMS iteration operators as

$$T_{\text{BRAS},n}^{(\nu)}(A_n) = I - \sum_{i=1}^{\nu} \hat{R}_i^T A_i^{-1} R_i A_n \quad (18)$$

and

$$T_{\text{BRMS},n}^{(\nu)}(A_n) = \prod_{i=\nu}^1 \left( I - \hat{R}_i^T A_i^{-1} R_i A_n \right), \quad (19)$$

$\hat{R}_i = \tilde{R}_i$  if  $i \in \mathcal{OV}$  and  $\hat{R}_i = R_i$  if  $i \notin \mathcal{OV}$ .

**Remark 2.4.** When a real symmetric (or Hermitian) problem is considered, it is a good numerical choice to preserve the real symmetry (or the Hermitian character) in the design of a preconditioner. In this spirit, the symmetrized version of the RAS iteration matrices is defined as

$$T_{\text{BRAS-sym},n}^{(\nu)}(A_n) = I - \sum_{i=1}^{\nu} \hat{R}_i^T A_i^{-1} \hat{R}_i A_n, \quad (20)$$

with  $\hat{R}_i = D_i R_i$  such that  $\sum_{i=1}^{\nu} \hat{R}_i^T R_i$  is the identity and  $D_i$  are diagonal. Unfortunately, by considering the corre-

sponding expression  $\prod_{i=\nu}^1 \left( I - \hat{R}_i^T A_i^{-1} \hat{R}_i A_n \right)$ , we obtain a variation of the RMS iteration matrices which are still non-symmetric, while the formulation

$$T_{\text{BRMS-sym},n}^{(\nu)}(A_n) = T^T T, \quad T = T_{\text{BRMS},n}^{(\nu)}(A_n) \quad (21)$$

is.

In all the previous reasoning, in order to apply the GLT theory, the diagonal weight matrices  $D_i$ ,  $i = 1, \dots, \nu$ , are chosen as diagonal sampling matrices; see Section 3.

### 3 Overview of the Theory of GLT Sequences

In the present section, we provide a concise overview of the main tool that we use in this paper, i.e., the theory of GLT matrix-sequences, which is instrumental in analyzing the spectral distribution of additive and multiplicative Schwarz methods and their variants, including the restricted versions. For brevity, we present only the results that are directly needed in this work. For readers new to the subject, we refer to [32, 33, 29], while more advanced treatments can be found in [6, 7, 8, 30, 31].

**Singular Value and Spectral Distribution of a Sequence of Matrices.** Let  $\mu_k$  denote the Lebesgue measure on  $\mathbb{R}^k$ . Throughout this paper, standard terminology from measure theory (such as "measurable set", "measurable function", "a.e.", etc.) always refers to the Lebesgue measure. A matrix-valued function

$$f : D \subset \mathbb{R}^k \longrightarrow \mathbb{C}^{s \times s}$$

is said to be measurable (respectively, continuous, continuous a.e., in  $\mathbb{L}^1(D)$ , etc.) if each of its components

$$f_{ij} : D \longrightarrow \mathbb{C}, \quad i, j = 1, \dots, s,$$

is measurable (respectively, continuous, continuous a.e., in  $\mathbb{L}^1(D)$ , etc.). For every  $x, y \in \mathbb{R}$ , define  $x \wedge y = \min(x, y)$ . We denote by  $C_c(\mathbb{C})$  (respectively,  $C_c(\mathbb{R})$ ) the space of complex-valued (respectively, real-valued) functions with compact support. The singular values of a matrix  $A \in \mathbb{C}^{m \times n}$  are denoted by  $\sigma_i(A)$ ,  $i = 1, \dots, m \wedge n$ , and the eigenvalues of a matrix  $A \in \mathbb{C}^{m \times m}$  are denoted by  $\lambda_i(A)$ ,  $i = 1, \dots, m$ . The spectrum of a matrix  $A \in \mathbb{C}^{m \times m}$  is denoted by  $\Lambda(A)$ . By definition, a sequence of matrices is a sequence of the form  $\{A_n\}_n$ , where  $n$  varies over an infinite subset of  $\mathbb{N}$ , and each  $A_n$  is of size  $d_n \times e_n$  with both  $d_n$  and  $e_n$  tending to  $\infty$  as  $n \rightarrow \infty$ .

**Definition 3.1 (Singular value and spectral distribution of a sequence of matrices).**

- Let  $\{A_n\}_n$  be a sequence of matrices with  $A_n$  of size  $d_n \times e_n$ , and let  $f : D \subset \mathbb{R}^k \rightarrow \mathbb{C}^{s \times t}$  be measurable with  $0 < \mu_k(D) < \infty$ .

We say that  $\{A_n\}_n$  has a *singular value distribution* described by  $f$ , and we write

$$\{A_n\}_n \sim_{\sigma} f,$$

if

$$\lim_{n \rightarrow \infty} \frac{1}{d_n \wedge e_n} \sum_{i=1}^{d_n \wedge e_n} F(\sigma_i(A_n)) = \frac{1}{\mu_k(D)} \int_D \left( \frac{1}{s \wedge t} \sum_{i=1}^{s \wedge t} F(\sigma_i(f(x))) \right) dx, \quad \forall F \in C_c(\mathbb{R}).$$

- Let  $\{A_n\}_n$  be a sequence of square matrices with  $A_n$  of size  $d_n \times d_n$ , and let  $f : D \subset \mathbb{R}^k \rightarrow \mathbb{C}^{s \times s}$  be measurable with  $0 < \mu_k(D) < \infty$ .

We say that  $\{A_n\}_n$  has a *spectral (or eigenvalue) distribution* described by  $f$ , and we write

$$\{A_n\}_n \sim_{\lambda} f,$$

if

$$\lim_{n \rightarrow \infty} \frac{1}{d_n} \sum_{i=1}^{d_n} F(\lambda_i(A_n)) = \frac{1}{\mu_k(D)} \int_D \left( \frac{1}{s} \sum_{i=1}^s F(\lambda_i(f(x))) \right) dx, \quad \forall F \in C_c(\mathbb{C}).$$

For the well-posedness of (3.1), we require the following lemma.

**Lemma 3.2.** Let  $f : D \subseteq \mathbb{R}^k \rightarrow \mathbb{C}^{s \times s}$  be a measurable function, and let  $g : \mathbb{C}^s \rightarrow \mathbb{C}$  be continuous and symmetric in its  $s$  arguments, that is,

$$g(\lambda_1, \dots, \lambda_s) = g(\lambda_{\rho(1)}, \dots, \lambda_{\rho(s)}) \quad \text{for all permutations } \rho \text{ of } \{1, \dots, s\}.$$

Then, the mapping

$$x \mapsto g(\lambda_1(f(x)), \dots, \lambda_s(f(x)))$$

is well-defined (independently of the ordering of the eigenvalues of  $f(x)$ ) and measurable.

As a consequence:

- the mapping  $x \mapsto g(\sigma_1(f(x)), \dots, \sigma_s(f(x)))$  is measurable;
- for every continuous function  $F : \mathbb{C} \rightarrow \mathbb{C}$ , the mappings

$$x \mapsto \sum_{i=1}^s F(\lambda_i(f(x))) \quad \text{and} \quad x \mapsto \sum_{i=1}^s F(\sigma_i(f(x)))$$

are measurable;

- for all  $p \in [1, \infty]$ , the mapping  $x \mapsto \|f(x)\|_p$  is measurable.

**Informal meaning of the singular value and eigenvalue distribution** (3.1). Assume that  $f$  admits  $s$  eigenvalue functions  $\lambda_i(f(x))$ ,  $i = 1, \dots, s$ , which are continuous almost everywhere on  $D$ . Then, the eigenvalues of  $A_n$ , except possibly for  $o(d_n)$  outliers, can be partitioned into  $s$  subsets of approximately equal cardinality. For sufficiently large  $n$ , the eigenvalues in the  $i$ -th subset are approximately equal to the samples of the  $i$ -th eigenvalue function  $\lambda_i(f(x))$  evaluated on a uniform grid over the domain  $D$ ,  $i = 1, \dots, s$ .

For example:

- If  $k = 1$ ,  $d_n = ns$ ,  $f$  is continuous,  $D = [a, b]$ , and assuming there are no outliers, then the eigenvalues of  $A_n$  are approximately given by

$$\lambda_i \left( f \left( a + \frac{j(b-a)}{n} \right) \right), \quad j = 1, \dots, n, \quad i = 1, \dots, s,$$

for sufficiently large  $n$ .

- If  $k = 2$ ,  $d_n = n^2 s$ ,  $f$  is continuous,  $D = [a_1, b_1] \times [a_2, b_2]$ , and assuming there are no outliers, then the eigenvalues of  $A_n$  are approximately given by

$$\lambda_i \left( f \left( a_1 + \frac{j_1(b_1-a_1)}{n}, a_2 + \frac{j_2(b_2-a_2)}{n} \right) \right), \quad j_1, j_2 = 1, \dots, n, \quad i = 1, \dots, s,$$

for sufficiently large  $n$ .

The same interpretation extends naturally to higher dimensions,  $k \geq 3$ , and to more general domains  $D$  with  $\mu_k(D) \in (0, \infty)$ : of course for more general domains  $D$  we have to compare with uniform samplings and hence we necessarily need that  $D$  is measurable according to Peano-Jordan i.e. its characteristic function is Riemann integrable; see e.g. [50, pp. 398–399]. An entirely analogous reasoning applies to the singular value distribution as well.

**Zero-distributed sequences.** A *zero-distributed sequence* is a sequence of matrices  $\{Z_n\}_n$  such that  $\{Z_n\}_n \sim_\sigma 0$ , i.e.,

$$\lim_{n \rightarrow \infty} \frac{1}{d_n \wedge e_n} \sum_{i=1}^{d_n \wedge e_n} F(\sigma_i(Z_n)) = F(0), \quad \forall F \in C_c(\mathbb{R}),$$

where  $d_n \times e_n$  is the size of  $Z_n$ .

**Toeplitz sequences.** Let  $f : [-\pi, \pi] \rightarrow \mathbb{C}^{s \times s}$  be a function in  $L^1([-\pi, \pi])$ . Its Fourier coefficients  $\{f_k\}_{k \in \mathbb{Z}}$  are defined by

$$f_k = \frac{1}{2\pi} \int_{-\pi}^{\pi} f(\theta) e^{-ik\theta} d\theta \in \mathbb{C}^{s \times s}, \quad k \in \mathbb{Z}, \quad (22)$$

where the integrals are computed componentwise.

The  $n$ -th (block) Toeplitz matrix generated by  $f$  is the  $ns \times ns$  matrix  $T_n(f)$  defined as

$$T_n(f) = [f_{i-j}]_{i,j=1}^n.$$

Any sequence of matrices of the form  $\{T_{d_n}(f)\}_n$ , with  $d_n \rightarrow \infty$  and  $f : [-\pi, \pi] \rightarrow \mathbb{C}^{s \times s}$  in  $L^1([-\pi, \pi])$ , is referred to as a *(block) Toeplitz sequence* generated by  $f$ .

**Sequences of diagonal sampling matrices.** Let  $a : [0, 1] \rightarrow \mathbb{C}^{s \times s}$ . The  $n$ -th (block) diagonal sampling matrix generated by  $a$  is the  $ns \times ns$  (block) diagonal matrix  $D_n(a)$  defined as

$$D_n(a) = \text{diag}(\{a(i/n)\}_{i=1}^n).$$

Any sequence of matrices of the form  $\{D_{d_n}(a)\}_n$ , with  $d_n \rightarrow \infty$  and  $a : [0, 1] \rightarrow \mathbb{C}^{s \times s}$ , is referred to as a *sequence of (block) diagonal sampling matrices generated by a*.

The construction of the GLT sequences is based on the notion of approximating class of sequences. Recently, this notion has been revisited in order to handle in a natural way also the case of approximations of PDEs on either moving or unbounded domains; see [1].

**GLT Sequences.** In the current section, we collect the properties of GLT sequences that are needed in this paper. Throughout this paper, we denote by  $I_s$  the  $s \times s$  identity matrix.

Before formulating these properties, we introduce some notation and terminology.

Throughout this paper, we denote by  $O_{s,t}$  the  $s \times s$  zero matrix. The matrix  $O_{s,s}$  is denoted by  $O_s$ . If the size is clear from the context, we often write  $O$  instead of  $O_{s,t}$  or  $O_s$ . If  $A$  is a matrix, we denote by  $A^\dagger$  the Moore–Penrose pseudoinverse of  $A$ . For our purposes, it is relevant that  $A^\dagger = A^{-1}$  whenever  $A$  is invertible. For more details on the pseudoinverse, see [37]. The properties of GLT sequences that we need in this paper are listed below; for the corresponding proofs, see [8].

**GLT0\*.** Let  $\{X_n\}_n$  be a sequence of matrices, with  $X_n$  of size  $d_n s \times d_n s$  for some fixed positive integer  $s$  and some positive integer sequence  $\{d_n\}_n$  tending to  $\infty$ , and let  $\kappa, \xi : [0, 1] \times [-\pi, \pi] \rightarrow \mathbb{C}^{s \times s}$  be measurable.

- If  $\{X_n\}_n \sim_{\text{GLT}} \kappa$  and  $\kappa = \xi$  a.e., then  $\{X_n\}_n \sim_{\text{GLT}} \xi$ .
- If  $\{X_n\}_n \sim_{\text{GLT}} \kappa$  and  $\{X_n\}_n \sim_{\text{GLT}} \xi$ , then  $\kappa = \xi$  a.e.

**GLT1\*.** Let  $\{X_n\}_n$  be a sequence of matrices, with  $X_n$  of size  $d_n s \times d_n s$  for some fixed positive integers  $s$  and some positive integer sequence  $\{d_n\}_n$  tending to  $\infty$ , and let  $\kappa : [0, 1] \times [-\pi, \pi] \rightarrow \mathbb{C}^{s \times s}$  be measurable.

- If  $\{X_n\}_n \sim_{\text{GLT}} \kappa$ , then  $\{X_n\}_n \sim_{\sigma} \kappa$ .
- If  $\{X_n\}_n \sim_{\text{GLT}} \kappa$  and the matrices  $X_n$  are Hermitian, then  $\kappa$  is Hermitian a.e., and  $\{X_n\}_n \sim_{\lambda} \kappa$ .

**GLT2\*.** Let  $s$  be a positive integer and let  $\{d_n\}_n$  be a positive integer sequence tending to  $\infty$ . Then,

- $\{T_{d_n}(f)\}_n \sim_{\text{GLT}} \kappa(x, \theta) = f(\theta)$  if  $f : [-\pi, \pi] \rightarrow \mathbb{C}^{s \times s}$  belongs to  $L^1([-\pi, \pi])$ ;
- $\{D_{d_n}(a)\}_n \sim_{\text{GLT}} \kappa(x, \theta) = a(x)$  if  $a : [0, 1] \rightarrow \mathbb{C}^{s \times s}$  is continuous a.e.;
- For every sequence of matrices  $\{Z_n\}_n$  with  $Z_n$  of size  $d_n s \times d_n s$ , we have  $\{Z_n\}_n \sim_{\text{GLT}} \kappa(x, \theta) = O_{s,t}$  if and only if  $\{Z_n\}_n \sim_{\sigma} 0$ .

**GLT3\*.** Let  $\{X_n\}_n, \{Y_n\}_n$  be sequences of matrices, with  $X_n, Y_n$  of size  $d_n s \times d_n s$  for some fixed positive integers  $s$  and some positive integer sequence  $\{d_n\}_n$  tending to  $\infty$ , and let  $\kappa, \xi : [0, 1] \times [-\pi, \pi] \rightarrow \mathbb{C}^{s \times s}$  be measurable. Suppose that  $\{X_n\}_n \sim_{\text{GLT}} \kappa$  and  $\{Y_n\}_n \sim_{\text{GLT}} \xi$ . Then,

- $\{X_n^*\}_n \sim_{\text{GLT}} \kappa^*$ ;
- $\{\alpha X_n + \beta Y_n\}_n \sim_{\text{GLT}} \alpha \kappa + \beta \xi$  for every  $\alpha, \beta \in \mathbb{C}$ ;
- $\{X_n Y_n\}_n \sim_{\text{GLT}} \kappa \xi$ ;
- $\{X_n^\dagger\}_n \sim_{\text{GLT}} \kappa^{-1}$  if  $\kappa$  is invertible a.e.;
- $\{f(X_n)\}_n \sim_{\text{GLT}} f(\kappa)$  if the matrices  $X_n$  are Hermitian and  $f : \mathbb{C} \rightarrow \mathbb{C}$  is continuous.

**GLT4\*.** Let  $\{X_n\}_n$  be a sequence of matrices, with  $X_n$  of size  $d_n s \times d_n s$  for some fixed positive integer  $s$  and some positive integer sequence  $\{d_n\}_n$  tending to  $\infty$ , and let  $\kappa : [0, 1] \times [-\pi, \pi] \rightarrow \mathbb{C}^{s \times s}$  be measurable. Suppose that there exists a sequence of sequences of matrices  $\{\{X_{n,m}\}_n\}_m$  with  $X_{n,m}$  of size  $d_n s \times d_n s$  such that

- $\{X_{n,m}\}_n \sim_{\text{GLT}} \kappa_m$  for some measurable  $\kappa_m : [0, 1] \times [-\pi, \pi] \rightarrow \mathbb{C}^{s \times s}$ ,
- $\kappa_m \rightarrow \kappa$  a.e. on  $[0, 1] \times [-\pi, \pi]$ ,
- $\{X_{n,m}\}_n \xrightarrow{\text{a.c.s.}} \{X_n\}_n$ .

Then,  $\{X_n\}_n \sim_{\text{GLT}} \kappa$ .

We remind that the topological notion of *approximating classes of sequences* (a.c.s.) is the cornerstone of an asymptotic approximation theory for sequences of matrices, that has been developed since the last 30 years and which represents the operative tool for building the GLT theory; see [49] for the first explicit definition, [30, Chapter 5] for a general treatment, and [1] for an extension and new results.

## 4 Schwarz Methods with GLT Preconditioning

The objective of this section is to introduce and discuss Theorem 4.2, which will be used in Section 5 to provide a theoretical justification for the efficiency of classical block preconditioners in Section 2 applied to GLT sequences. To establish this result, we first need the following lemma. Throughout this paper, we adopt the abbreviations HPD and HPSD to be positive definite and Hermitian positive semi-definite matrices, respectively.

**Lemma 4.1.** *Let  $\{A_n\}_n$  be a sequence of HPSD matrices, with  $A_n$  of size  $d_n s$  for some fixed positive integer  $s$  and some positive integer sequence  $\{d_n\}_n$  tending to  $\infty$ , and let  $\kappa : [0, 1] \times [-\pi, \pi] \rightarrow \mathbb{C}^{s \times s}$  be measurable. If  $\{A_n\}_n \sim_{GLT} \kappa$ , then  $\kappa$  is HPSD a.e.*

*Proof.* Since the matrices  $A_n$  are Hermitian, we know from **GLT1\***. that  $\kappa$  is Hermitian a.e. and  $\{A_n\}_n \sim_{\lambda} \kappa$ . Since the matrices  $A_n$  are positive semi-definite,  $\Lambda(A_n) \subset [0, \infty)$  for all  $n$ . Hence, by Lemma 2.1,  $\Lambda(\kappa) \subset [0, \infty)$  a.e. Thus,  $\kappa$  is HPD a.e.  $\square$

**Theorem 4.2.** *Let  $\{A_n\}_n$  be a sequence of Hermitian matrices, with  $A_n$  of size  $d_n s$  for some fixed positive integer  $s$  and some positive integer sequence  $\{d_n\}_n$  tending to  $\infty$ , and let  $\{P_n\}_n$  be a sequence of HPD matrices, with  $P_n$  of size  $d_n s$ . Suppose that  $\{A_n\}_n \sim_{GLT} \kappa$  and  $\{P_n\}_n \sim_{GLT} \xi$ , where  $\kappa, \xi : [0, 1] \times [-\pi, \pi] \rightarrow \mathbb{C}^{s \times s}$  are measurable and  $\xi$  is invertible a.e. Then, the sequence of preconditioned matrices  $P_n^{-1} A_n$  satisfies*

$$\{P_n^{-1} A_n\}_n \sim_{GLT} \xi^{-1} \kappa, \quad \{P_n^{-1} A_n\}_n \sim_{\sigma} \xi^{-1} \kappa, \quad \{P_n^{-1} A_n\}_n \sim_{\lambda} \xi^{-1} \kappa.$$

*Proof.* By Axiom **GLT3\***., fourth part, and by the assumptions, we know that  $\{P_n^{-1}\}_n \sim_{GLT} \xi^{-1}$  and hence by Axiom **GLT3\***., third part, it follows the first claim that is

$$\{P_n^{-1} A_n\}_n \sim_{GLT} \xi^{-1} \kappa.$$

Therefore the relation  $\{P_n^{-1} A_n\}_n \sim_{\sigma} \xi^{-1} \kappa$  is now a direct consequence of Axiom **GLT1\***., first part, and hence the second fact is proven.

Unfortunately, Axiom **GLT1\***., second part cannot be used because in general  $P_n^{-1} A_n$  fails to be Hermitian. However  $\{P_n^{-1} A_n\}_n \sim_{\lambda} \xi^{-1} \kappa$  if and only if  $\{P_n^{-1/2} A_n P_n^{-1/2}\}_n \sim_{\lambda} \xi^{-1/2} \kappa \xi^{-1/2}$ , since  $P_n^{-1} A_n$  is similar to  $P_n^{-1/2} A_n P_n^{-1/2}$  for every  $n$  and  $\xi^{-1} \kappa$  is similar to  $\xi^{-1/2} \kappa \xi^{-1/2}$  a.e. Now the proof is concluded since  $\{P_n^{-1/2} A_n P_n^{-1/2}\}_n \sim_{\lambda} \xi^{-1/2} \kappa \xi^{-1/2}$  because all the matrices are Hermitian and  $\{P_n^{-1/2} A_n P_n^{-1/2}\}_n \sim_{GLT} \xi^{-1/2} \kappa \xi^{-1/2}$  is a consequence of **GLT3\***., fifth part, with  $f(z) = z^{1/2}$ , followed by Axiom **GLT3\***., fourth part, and finally by invoking Axiom **GLT3\***., third part, two times.  $\square$

To establish this result, we first recall the fundamental concepts underlying the one-level GLT theory.

## 5 One-Level GLT Sequences

In the following, we restrict our attention to the one-level case of GLT sequences, corresponding to the setting  $s = t \geq 1$  introduced earlier. The statements and the mathematical derivations are done in the case of  $s = t = 1$ . The general case of  $s = t > 1$  is treated in Remark 5.3 and it is not academical since methods such as Discontinuous Galerkin, high order Finite Elements, Isogeometric Analysis with intermediate regularity, and hybrid methods lead to block structures and to matrix-valued GLT symbols [35, 23, 24, 36].

**Theorem 5.1.** *Let  $\nu \geq 1$ , be a fixed integer, and let  $\{d_n\}_n$  be a sequence of positive integers tending to  $\infty$ . For every  $n$ , let*

$$(n_1, \dots, n_{3\nu-2}) = (n_1(n), \dots, n_{3\nu-2}(n))$$

*be a partition of  $d_n$ . Assume that  $\{A_n\}_n \sim_{GLT} \kappa$  for some measurable function  $\kappa$ . Then*

$$\left\{ P_{\star, n}^{(\nu)}(A_n) \right\}_n \sim_{GLT} \kappa,$$

*where  $\star \in \{\text{BJ, BAS, BGS, BMS}\}$  and with  $\nu$  non-overlapping subdomains. Furthermore, under the same notations and under the assumption that  $\kappa$  is invertible a.e., we have*

$$\{P_n^{-1} A_n\}_n \sim_{GLT, \sigma} 1, \quad \{T_n = I_{d_n} - P_n^{-1} A_n\}_n \sim_{GLT, \sigma} 0$$

*with  $P_n = P_{\star, n}^{(\nu)}(A_n)$ . Finally  $\{P_n^{-1} A_n\}_n \sim_{\lambda} 1$  and  $\{T_n = I_{d_n} - P_n^{-1} A_n\}_n \sim_{\lambda} 0$  whenever both  $P_n$  and  $A_n$  are both positive definite.*

*Proof.* First of all we observe that the block Jacobi (BJ) preconditioning and the block Gauss Seidel (BGS) preconditioning coincide with the block additive Schwarz (BAS) and with the block multiplicative Schwarz (BMS) preconditioning, of course also in their restricted version, since there is no overlapping among the  $\nu$  subdomains; see Remark 2.1.

Hence the claimed results regarding the matrix-sequences  $\left\{P_{\star,n}^{(\nu)}(A_n)\right\}_n$  and  $\left\{P_n^{-1}A_n\right\}_n$  with  $P_n = P_{\star,n}^{(\nu)}(A_n)$  can be found in [34, Theorem 4.4 and Theorem 4.5] (also in the more general version of rectangular GLT symbols) and by Theorem 4.2 (see also [34, Remark 4.1]) for the preconditioned matrix-sequences.

It remains to consider the iteration matrix-sequences  $\left\{T_n = I_{d_n} - P_n^{-1}A_n\right\}_n$ . Now the relation  $\left\{T_n = I_{d_n} - P_n^{-1}A_n\right\}_n \sim_{\text{GLT}} 0$  is a consequence of Axiom **GLT3\***, second part and of Axiom **GLT2\***, first part, since  $T_n(1)$  is the identity matrix, while Axiom **GLT1\*** leads to  $\left\{T_n = I_{d_n} - P_n^{-1}A_n\right\}_n \sim_{\sigma} 0$ . Finally, following Theorem 4.2, again by Axiom **GLT1\***,  $\left\{T_n = I_{d_n} - P_n^{-1}A_n\right\}_n \sim_{\lambda} 0$  when  $A_n$  is positive definite for any and in the block Jacobi setting since  $P_n$  is also positive definite.  $\square$

The overlapping is definitely more involved and for that we need new ideas as already indicated in Remark 2.1. For making them crystal clear, the proof of the subsequent three theorems contains all the details in the simplest case of two subdomains i.e.  $\nu = 2$ . Theorem 5.2 contains a negative result concerning the block additive Schwarz preconditioning with overlapping, while its restricted version shows again the desired behavior. As anticipated in Remark 2.2, the block multiplicative Schwarz does need to be corrected.

**Theorem 5.2.** *Let  $\nu \geq 1$ , be a fixed integer, and let  $\{d_n\}_n$  be a sequence of positive integers tending to  $\infty$ . For every  $n$ , let*

$$(n_1, \dots, n_{3\nu-2}) = (n_1(n), \dots, n_{3\nu-2}(n))$$

*be a partition of  $d_n$ . Assume that  $\{A_n\}_n \sim_{\text{GLT}} \kappa$  for some measurable function  $\kappa$ , invertible a.e. Then*

$$\left\{P_{\star,n}^{(\nu)}(A_n)\right\}_n \sim_{\text{GLT}} \psi = \kappa \sum_{i=1}^{\nu} a_i,$$

*where  $\star = \text{BAS}$ , with  $\nu$  subdomains with overlapping and with  $a_i$  being the characteristic function of  $\Omega_i$ ,  $i = 1, \dots, \nu$ . Furthermore, under the same notations, we have*

$$\left\{P_n^{-1}A_n\right\}_n \sim_{\text{GLT}, \sigma} \frac{\kappa}{\psi}, \quad \left\{T_n = I_{d_n} - P_n^{-1}A_n\right\}_n \sim_{\text{GLT}, \sigma} 1 - \frac{\kappa}{\psi}$$

*with  $P_n = P_{\star,n}^{(\nu)}(A_n)$  and  $\left\|1 - \frac{\kappa}{\psi}\right\|_{\infty} = \frac{1}{2}$ .*

*Proof.* Following (13), we have

$$T_{\text{BAS},n}^{(\nu=2)}(A_n) = I - \sum_{i=1}^2 R_i^T A_i^{-1} R_i A_n$$

where

$$R_1^T A_1^{-1} R_1 = \begin{bmatrix} A_1^{-1} & O \\ O & O \end{bmatrix} = \left[ \text{BlockDiag}_{\hat{d}_1(n), d_n - \hat{d}_1(n)}(A_n) \right]^{-1} \begin{bmatrix} I_{\hat{d}_1(n)} & O \\ O & O \end{bmatrix}$$

$\hat{d}_1(n) = d_1(n) + n_3$ , and

$$R_2^T A_2^{-1} R_2 = \begin{bmatrix} O & O \\ O & A_2^{-1} \end{bmatrix} = \left[ \text{BlockDiag}_{d_n - \hat{d}_2(n), \hat{d}_2(n)}(A_n) \right]^{-1} \begin{bmatrix} O & O \\ O & I_{\hat{d}_2(n)} \end{bmatrix}$$

$\hat{d}_2(n) = d_2(n) + n_2$ , with  $d_n = d_1(n) + d_2(n)$ ,  $d_1(n) = n_1 + n_2$ ,  $d_2(n) = n_3 + n_4$ , so that  $d_n - \hat{d}_1(n) = n_4$  and  $d_n - \hat{d}_2(n) = n_1$ . The right-hand sides of the latter two equations is very informative from the GLT viewpoint since

$$R_1^T A_1^{-1} R_1 = \left[ \text{BlockDiag}_{\hat{d}_1(n), d_n - \hat{d}_1(n)}(A_n) \right]^{-1} D_n(a_1), \quad R_2^T A_2^{-1} R_2 = \left[ \text{BlockDiag}_{d_n - \hat{d}_2(n), \hat{d}_2(n)}(A_n) \right]^{-1} D_n(a_2),$$

$a_i$  being the characteristic function of the domain  $\Omega_i$ ,  $i = 1, 2$ ,  $D_n(a_i)$ ,  $i = 1, 2$ , as in Axiom **GLT2\***, second part, for which

$$\{D_n(a_i)\}_n \sim_{\text{GLT}} a_i, \quad i = 1, 2.$$

Since  $\{A_n\}_n \sim_{\text{GLT}} \kappa$ , by Theorem [34, Theorem 4.4] we deduce

$$\left\{ \text{BlockDiag}_{\hat{d}_1(n), d_n - \hat{d}_1(n)}(A_n) \right\}_n \sim_{\text{GLT}} \kappa, \quad \left\{ \text{BlockDiag}_{d_n - \hat{d}_2(n), \hat{d}_2(n)}(A_n) \right\}_n \sim_{\text{GLT}} \kappa.$$

Therefore, using Axiom **GLT3\***., fourth part, and Axiom **GLT3\***., third part, we obtain

$$\{R_1^T A_1^{-1} R_1\}_n \sim_{\text{GLT}} a_1 \kappa^{-1}, \quad \{R_2^T A_2^{-1} R_2\}_n \sim_{\text{GLT}} a_2 \kappa^{-1}$$

so that  $\left\{ \sum_{i=1}^2 R_i^T A_i^{-1} R_i A_n \right\}_n \sim_{\text{GLT}} a_1 + a_2$ , by invoking Axiom **GLT3\***., second part and third part. Hence

$$\left\{ P_{\star,n}^{(\nu)}(A_n) \right\}_n \sim_{\text{GLT}} \psi = \kappa(a_1 + a_2)$$

$\{P_n^{-1} A_n\}_n \sim_{\text{GLT}} \frac{1}{a_1 + a_2} = \frac{\kappa}{\psi}$ ,  $\{T_n = I_{d_n} - P_n^{-1} A_n\}_n \sim_{\text{GLT}} 1 - \frac{1}{a_1 + a_2} = 1 - \frac{\kappa}{\psi}$ . Now the use of Axiom 1 concludes the proof for the BAS method with  $\nu = 2$ , since  $a_1(1) + a_2(x) = 1$  for  $x \notin \Omega_1 \cap \Omega_2$  and  $a_1(1) + a_2(x) = 2$  for  $x \in \Omega_1 \cap \Omega_2$  so that  $\left\| 1 - \frac{\kappa}{\psi} \right\|_\infty = \frac{1}{2}$ .

The case of  $\nu > 2$  subdomains follows the same steps, taking into consideration the admissibility conditions in Remark 2.3.  $\square$

**Theorem 5.3.** *Let  $\nu \geq 1$ , be a fixed integer, and let  $\{d_n\}_n$  be a sequence of positive integers tending to  $\infty$ . For every  $n$ , let*

$$(n_1, \dots, n_{3\nu-2}) = (n_1(n), \dots, n_{3\nu-2}(n))$$

*be a partition of  $d_n$ . Assume that  $\{A_n\}_n \sim_{\text{GLT}} \kappa$  for some measurable function  $\kappa$ , invertible a.e. Then*

$$\left\{ P_{\star,n}^{(\nu)}(A_n) \right\}_n \sim_{\text{GLT}} \kappa,$$

*where  $\star = \text{BMS}$ , with  $\nu$  subdomains with overlapping and with  $a_i$  being the characteristic function of  $\Omega_i$ ,  $i = 1, \dots, \nu$ . Furthermore, under the same notations, we have*

$$\{P_n^{-1} A_n\}_n \sim_{\text{GLT},\sigma} 1, \quad \{T_n = I_{d_n} - P_n^{-1} A_n\}_n \sim_{\text{GLT},\sigma} 0$$

*with  $P_n = P_{\star,n}^{(\nu)}(A_n)$ .*

*Proof.* For the multiplicative version we invoke the explicit expression in (14). In fact, the proof uses the same arguments as in Theorem 5.2, using again the  $\star$ -algebra structure of the GLT matrix-sequences. Looking indeed at the related matrix-sequence  $\{P_n^{-1}\}_n$  as in (12), the GLT symbol is

$$(1 - (1 - a_2 \kappa^{-1} \kappa) (1 - a_1 \kappa^{-1} \kappa)) \kappa^{-1} = (a_1 + a_2 - a_1 a_2) \kappa^{-1} = \kappa^{-1},$$

since  $a_1 + a_2 - a_1 a_2 = 1$  both in the overlapping and non-overlapping setting.

The case of  $\nu > 2$  subdomains follows the same steps, taking into consideration the admissibility conditions in Remark 2.3.  $\square$

**Theorem 5.4.** *Let  $\nu \geq 1$ , be a fixed integer, and let  $\{d_n\}_n$  be a sequence of positive integers tending to  $\infty$ . For every  $n$ , let*

$$(n_1, \dots, n_{3\nu-2}) = (n_1(n), \dots, n_{3\nu-2}(n))$$

*be a partition of  $d_n$ . Assume that  $\{A_n\}_n \sim_{\text{GLT}} \kappa$  for some measurable function  $\kappa$ . Then*

$$\left\{ P_{\star,n}^{(\nu)}(A_n) \right\}_n \sim_{\text{GLT}} \kappa,$$

*where  $\star \in \{\text{BRAS, BRMS}\}$  and with  $\nu$  subdomains with overlapping. Furthermore, under the same notations and under the assumption that  $\kappa$  is invertible a.e., we have*

$$\{P_n^{-1} A_n\}_n \sim_{\text{GLT},\sigma} 1, \quad \{T_n = I_{d_n} - P_n^{-1} A_n\}_n \sim_{\text{GLT},\sigma} 0$$

*with  $P_n = P_{\star,n}^{(\nu)}(A_n)$ . Finally  $\{P_n^{-1} A_n\}_n \sim_{\lambda} 1$  and  $\{T_n = I_{d_n} - P_n^{-1} A_n\}_n \sim_{\lambda} 0$  whenever both  $P_n$  and  $A_n$  are both positive definite.*

*Proof.* As for Theorem 5.2, we start by considering the case of two subdomains, i.e.,  $\nu = 2$ . The proof is contained in the following observation: the action of the restricted operators changes  $a_1$  into  $\hat{a}_1$  and  $a_2$  into  $\hat{a}_2$ ,  $\hat{a}_i$ ,  $i = 1, 2$ , being the characteristic functions of  $\Omega_i$ ,  $S_i$ ,  $i = 1, 2$ ,  $S_1 \cup S_2 = \Omega_1 \cap \Omega_2$ ,  $S_1 \cap S_2 = \emptyset$ . Therefore  $\psi = \kappa \sum_{i=1}^{\nu} \hat{a}_i$  coincides with  $\kappa$ , the sum  $\sum_{i=1}^{\nu} \hat{a}_i$  becoming again a partition of the unity as in the non-overlapping case.

More in detail, let  $\{A_n\}_n \sim_{\text{GLT}} \kappa$  for some measurable function  $\kappa$ . Following (13), we have

$$T_{\text{BAS},n}^{(\nu=2)}(A_n) = I - \sum_{i=1}^2 \hat{R}_i^T A_i^{-1} R_i A_n$$

where

$$\hat{R}_1^T A_1^{-1} R_1 = \begin{bmatrix} I_{d_1(n)} & O \\ O & O \end{bmatrix} \begin{bmatrix} A_1^{-1} & O \\ O & O \end{bmatrix} = \left[ \text{BlockDiag}_{\hat{d}_1(n), d_n - \hat{d}_1(n)}(A_n) \right]^{-1} \begin{bmatrix} I_{\hat{d}_1(n)} & O \\ O & O \end{bmatrix}$$

$\hat{d}_1(n) = d_1(n) + n_3$ , and

$$\hat{R}_2^T A_2^{-1} R_2 = \begin{bmatrix} O & O \\ O & I_{d_2(n)} \end{bmatrix} \begin{bmatrix} O & O \\ O & A_2^{-1} \end{bmatrix} = \left[ \text{BlockDiag}_{d_n - \hat{d}_2(n), \hat{d}_2(n)}(A_n) \right]^{-1} \begin{bmatrix} O & O \\ O & I_{\hat{d}_2(n)} \end{bmatrix}$$

$\hat{d}_2(n) = d_2(n) + n_2$ , with  $d_n = d_1(n) + d_2(n)$ ,  $d_1(n) = n_1 + n_2$ ,  $d_2(n) = n_3 + n_4$ , so that  $d_n - \hat{d}_1(n) = n_4$  and  $d_n - \hat{d}_2(n) = n_1$ . The right-hand sides of the latter two equations are very useful for deducing the GLT structure since

$$\begin{aligned} \hat{R}_1^T A_1^{-1} R_1 &= D_n(\hat{a}_1) \left[ \text{BlockDiag}_{\hat{d}_1(n), d_n - \hat{d}_1(n)}(A_n) \right]^{-1} D_n(a_1), \\ \hat{R}_2^T A_2^{-1} R_2 &= D_n(\hat{a}_2) \left[ \text{BlockDiag}_{d_n - \hat{d}_2(n), \hat{d}_2(n)}(A_n) \right]^{-1} D_n(a_2), \end{aligned}$$

$a_i$  being the characteristic function of the domain  $\Omega_i$ ,  $i = 1, 2$ ,  $D_n(a_i)$ ,  $D_n(\hat{a}_i)$ ,  $i = 1, 2$ , as in Axiom **GLT2\***., second part, for which

$$\{D_n(a_i)\}_n \sim_{\text{GLT}} a_i, \quad \{D_n(\hat{a}_i)\}_n \sim_{\text{GLT}} \hat{a}_i, \quad i = 1, 2.$$

Since  $\{A_n\}_n \sim_{\text{GLT}} \kappa$ , by Theorem [34, Theorem 4.4] we deduce

$$\left\{ \text{BlockDiag}_{\hat{d}_1(n), d_n - \hat{d}_1(n)}(A_n) \right\}_n \sim_{\text{GLT}} \kappa, \quad \left\{ \text{BlockDiag}_{d_n - \hat{d}_2(n), \hat{d}_2(n)}(A_n) \right\}_n \sim_{\text{GLT}} \kappa.$$

Therefore, using Axiom **GLT3\***., fourth part, and Axiom **GLT3\***., third part, we obtain

$$\{\hat{R}_1^T A_1^{-1} R_1\}_n \sim_{\text{GLT}} \hat{a}_1 a_1 \kappa^{-1} = \hat{a}_1 \kappa^{-1}, \quad \{\hat{R}_2^T A_2^{-1} R_2\}_n \sim_{\text{GLT}} \hat{a}_2 a_2 \kappa^{-1} = \hat{a}_2 \kappa^{-1}$$

so that  $\left\{ \sum_{i=1}^2 \hat{R}_i^T A_i^{-1} R_i A_n \right\}_n \sim_{\text{GLT}} \hat{a}_1 + \hat{a}_2 = 1$ , by invoking Axiom **GLT3\***., second part and third part. As a consequence, we have

$$\left\{ P_{\star,n}^{(\nu)}(A_n) \right\}_n \sim_{\text{GLT}} \kappa$$

and consequently  $\{P_n^{-1} A_n\}_n \sim_{\text{GLT}} 1$ ,  $\{T_n = I_{d_n} - P_n^{-1} A_n\}_n \sim_{\text{GLT}} 0$ . Now the use of Axiom 1 concludes the proof for the BAS method with  $\nu = 2$ .

Due to the admissibility conditions in Remark 2.3, the case of  $\nu > 2$  subdomains can be treated in the same way since the overlapping holds at most for consecutive subdomains  $\Omega_i$  and  $\Omega_{i+1}$  with  $i \in \mathcal{OV}$ : hence the proof with  $\nu > 2$  is given by iterating the same reasoning as for  $\nu = 2$  for every  $i \in \mathcal{OV}$ .  $\square$

**Remark 5.1.** Following the above theorem, block Jacobi, block Gauss–Seidel, as well as block additive and block multiplicative preconditioners (with the proper corrections) are expected to be efficient for GLT sequences, with the additive and multiplicative variants generally showing superior performance.

Let  $\{A_n\}_n \sim_{\text{GLT}} \kappa$ , where  $A_n$  is a square matrix of size  $d_n \times d_n$  and  $\kappa : [0, 1] \times [-\pi, \pi] \rightarrow \mathbb{C}$  is measurable. Let  $(n_1, \dots, n_{3\nu-2}) = (n_1(n), \dots, n_{3\nu-2}(n))$  be a partition of  $d_n$  into a fixed number of blocks  $\nu$ , independent of  $n$ . Then any block preconditioner  $P_{\star,n}^{(\nu)}$  of Jacobi, Gauss–Seidel, restricted additive, or multiplicative type satisfies

$$\{P_{\star,n}^{(\nu)}(A_n)\}_n \sim_{\text{GLT}} \kappa. \quad (23)$$

Assuming that  $P_{\star,n}^{(\nu)}$  are invertible and that  $\kappa$  is invertible almost everywhere, equation (23) together with GLT property **GLT3\*** (for  $s = 1$ ) yield

$$\{(P_{\star,n}^{(\nu)})^{-1} A_n\}_n \sim_{\text{GLT}} 1.$$

This spectral distribution holds whenever  $A_n$  are HPD and  $\kappa$  is invertible almost everywhere. In this case, the preconditioners  $P_{\star,n}^{(\nu)}$  are also HPD (when  $\star \in \{BJ, BAS\}$ ), and the spectral distribution follows from Theorem 4.2. Importantly, these spectral distributions correspond to the (weak, in the non-overlapping case for Jacobi/Gauss-Seidel) clustering of the eigenvalues at 1 for  $P_{BRAS,BGS,BMS,BRMS,n}^{(\nu)}$  (also  $P_{BAS,n}^{(\nu)}$  in the non-overlapping case). Therefore, in view of the convergence properties of preconditioned Krylov methods,  $P_{\star,n}^{(\nu)}$  are expected to be efficient preconditioners for  $A_n$ , also in view of the convergence theorems for (preconditioned) Krylov solvers in presence of distribution results for (preconditioned) matrix-sequences [11, 42]. Notice that these convergence results can be combined with the standard convergence theory either of block Jacobi methods for e.g. block diagonal dominant and irreducible matrices or of block Gauss-Seidel methods e.g. for positive definite coefficient matrices.

Numerical experiments supporting this claim are presented in the following Section.

**Remark 5.2.** The importance of the partition of unity has becoming very important for proving that the preconditioned matrix-sequence has the very same GLT symbol as the original matrix-sequence: this is very clear in the proof of Theorem 5.4.

However we must emphasize that the latter represents a guiding tool for a general recipe, when deciding restriction operators as in Remark 2.4: in fact the weight matrices can be imagined as sampling matrices whose matrix-sequences are automatically GLT matrix-sequences, whose related GLT symbols are designed with the constraint of the partition of unity (compare the proof of Theorem 5.4 and Remark 2.4). This flexibility represents an important direction to be explored more in order to defined new variations of Block Schwarz additive and multiplicative methods.

**Remark 5.3.** In Theorems 5.1, 5.2, 5.3, 5.4 we have considered only the case of scalar-valued GLT symbols, even if the theory is available in full generality [8, 9, 35, 34] as also reported in Lemma 4.1 and Theorem 4.2.

However, when considering either a Galerkin or collocation approach in Isogeometric Analysis with intermediate regularity, when considering hybrid methods, Discontinuous Galerkin or high order Finite Elements, we end up with matrix structures whose related matrix-sequences are of GLT nature with matrix-valued GLT symbols [35, 23, 24, 36]. More precisely the size of the matrix-valued symbols is equal  $\mu(p - k)^d$  (see the discussion in the introduction of [1] and [8, 9, 35, 23, 24, 36]), where  $d$  is the dimensionality of the physical domain,  $p$  is the polynomial degree,  $k$  is the global regularity of the numerical solution,  $\mu$  the number of PDEs when systems of PDEs are considered in connection with the blocking approach [4, 5, 2, 3, 13]. Furthermore, also general domains and graded meshes can be considered as discussed in [12, 13, 50, 50].

However, looking back at Theorems 5.1, 5.2, 5.3, 5.4 the generalization to matrix-valued symbols is plain since the characteristic functions used in deriving the results are scalar-valued in nature and hence they commute with any matrix-valued symbol. In the subsequent numerical section few numerical tests with matrix-valued symbols are considered for showing the adaptability of our theoretical analysis.

## 6 Numerical experiments

In this section, we demonstrate the efficiency of block Jacobi/Gauss-Seidel and additive/multiplicative preconditioners for GLT sequences, in agreement with the predictions of Remark 5.1. Each example is presented following the procedure outlined below.

- (A) We fix a GLT sequence  $\{A_n\}_n \sim_{\text{GLT}} \kappa$ , where each  $A_n$  is an invertible square matrix of size  $n^d s \times n^d s$ , for some fixed positive integer  $s$ , and  $\kappa : [0, 1]^d \times [-\pi, \pi]^d \rightarrow \mathbb{C}^{s \times s}$  is a measurable matrix-valued function. In most of the examples we have  $s = d = 1$ , but we also consider the case of  $s \geq 2$  and that of  $d = 2$ .
- (B) The tables report, for increasing values of  $\nu, n$  and overlap size  $o$ , the number of iterations required to solve the linear system  $A_n x = \mathbf{1}$  with a tolerance of  $10^{-6}$ . Results are provided for both the preconditioned conjugate gradient (PCG) method with  $P_{\star,n}^{(\nu)}$  and the preconditioned GMRES (PGMRES) method. All solvers are initialized with the zero vector  $\mathbf{0}$ , and PGMRES is applied without restarting. Entries marked as "nac" indicate **cases that are not admissible**, this is because the overlap size  $o$  cannot exceed the size of the subdomains, in accordance with the admissibility conditions stated in Remark (2.3). The results clearly confirm the efficiency of Schwarz-type preconditioners in accelerating convergence for both iterative methods, with convergence improving as the overlap increases.

(C) For  $s > 1$ , we plot the graphs of selected continuous eigenvalue functions  $\lambda_i(f)$ ,  $i = 1, \dots, s$ , associated with the function  $f$ , together with the eigenvalues of the matrix  $A_n$ , for a selected value of  $n$ . The eigenvalues of  $A_n$  are subdivided into  $s$  distinct subsets of approximately equal cardinality. The eigenvalues in each subset are then positioned at the nodes of a uniform grid in  $[0, \pi]$ .

## 6.1 The 1D setting

**Example 6.1** (Full Toeplitz matrices). Consider the Toeplitz matrix  $A_n = T_n(f)$  generated by the symbol  $f(\theta) = |\theta|$ . The corresponding matrix sequence  $\{A_n\}_n$  satisfies  $\{A_n\}_n \sim_{GLT} f$ , by property **GLT2\***. For item (A), we fix the parameter  $s = 1$  and subsequently apply the procedure described in item (B). The resulting numerical results, obtained via various methods, are summarized in Tables 1–14.

Figure 2 provides a visual comparison of standard versus preconditioned GMRES. The left plot shows the residuals for unpreconditioned methods, while the right plot shows the residuals for preconditioned methods. The simulation is performed with matrix size  $n = 1280$ , number of subdomains  $\nu = 2$ , and overlap  $o = 30$ .

Figure 3 compares the eigenvalues for different block preconditioners with matrix size  $n = 40$ , number of subdomains  $\nu = 2$ , and overlap  $o = 10$ . The markers represent the eigenvalues of  $A_n$ ,  $P_n^{-1}$ , and  $P_n^{-1}A_n$  for each method, illustrating the clustering effect induced by the preconditioners and confirming the spectral distribution predictions based on GLT analysis.

Method	$\nu$	$n = 40$	$n = 80$	$n = 160$	$n = 320$	$n = 640$	$n = 1280$	$n = 2560$
CG	1	20	30	44	63	90	128	182
	1	20	30	44	63	90	128	182
	1	20	30	44	63	90	128	182
	1	20	30	44	63	90	128	182
PCG	2	5	6	6	6	7	7	7
	4	8	9	10	10	11	12	12
	8	12	13	14	16	17	18	19
	16	19	17	19	21	23	25	28
GMRES	1	20	45	80	147	303	624	1192
	1	20	45	80	147	303	624	1192
	1	20	45	80	147	303	624	1192
	1	20	45	80	147	303	624	1192
PGMRES	2	5	6	6	9	7	10	11
	4	8	12	10	15	16	19	18
	8	13	14	17	19	21	22	30
	16	20	18	21	23	27	30	36

Table 1: Number of iterations for CG and GMRES with  $P_{BL,n}^{(\nu)}(A_n)$ .

Method	$\nu$	$n = 40$	$n = 80$	$n = 160$	$n = 320$	$n = 640$	$n = 1280$	$n = 2560$
CG	1	20	30	44	63	90	128	182
	1	20	30	44	63	90	128	182
	1	20	30	44	63	90	128	182
	1	20	30	44	63	90	128	182
PCG	2	4	5	5	5	6	6	6
	4	8	8	9	9	9	10	11
	8	8	10	11	12	13	14	15
	16	nac	10	12	14	16	17	21
GMRES	1	20	45	80	147	303	624	1192
	1	20	45	80	147	303	624	1192
	1	20	45	80	147	303	624	1192
	1	20	45	80	147	303	624	1192
PGMRES	2	4	6	5	7	9	6	10
	4	8	10	10	10	12	14	16
	8	8	11	12	13	15	16	20
	16	nac	11	13	15	17	20	21

Table 2: Number of iterations for CG and GMRES with  $P_{BAS,n}^{(\nu)}(A_n)$ , overlap  $o = 5$ .

<b>Method</b>	$\nu$	$n = 40$	$n = 80$	$n = 160$	$n = 320$	$n = 640$	$n = 1280$	$n = 2560$
CG	1	20	30	44	63	90	128	182
	1	20	30	44	63	90	128	182
	1	20	30	44	63	90	128	182
	1	20	30	44	63	90	128	182
PCG	2	4	4	5	5	5	6	6
	4	6	8	8	9	9	9	10
	8	nac	9	11	11	12	13	14
	16	nac	nac	10	13	14	16	17
GMRES	1	20	45	80	147	303	624	1192
	1	20	45	80	147	303	624	1192
	1	20	45	80	147	303	624	1192
	1	20	45	80	147	303	624	1192
PGMRES	2	5	4	6	5	5	9	6
	4	7	8	11	10	10	12	14
	8	nac	9	13	16	12	15	17
	16	nac	nac	11	14	15	17	20

Table 3: Number of iterations for CG and GMRES with  $P_{BAS,n}^{(\nu)}(A_n)$ , with overlap  $o = 10$ .

<b>Method</b>	$\nu$	$n = 40$	$n = 80$	$n = 160$	$n = 320$	$n = 640$	$n = 1280$	$n = 2560$
CG	1	20	30	44	63	90	128	182
	1	20	30	44	63	90	128	182
	1	20	30	44	63	90	128	182
	1	20	30	44	63	90	128	182
PCG	2	nac	3	4	4	5	5	6
	4	nac	nac	8	8	8	9	9
	8	nac	nac	nac	10	11	11	13
	16	nac	nac	nac	nac	12	13	15
GMRES	1	20	45	80	147	303	624	1192
	1	20	45	80	147	303	624	1192
	1	20	45	80	147	303	624	1192
	1	20	45	80	147	303	624	1192
PGMRES	2	nac	3	4	4	5	5	7
	4	nac	nac	8	10	8	9	13
	8	nac	nac	nac	12	11	13	15
	16	nac	nac	nac	nac	13	15	16

Table 4: Number of iterations for CG and GMRES with  $P_{BAS,n}^{(\nu)}(A_n)$ , with overlap  $o = 30$ .

<b>Method</b>	$\nu$	$n = 40$	$n = 80$	$n = 160$	$n = 320$	$n = 640$	$n = 1280$	$n = 2560$
CG	1	20	30	44	63	90	128	182
	1	20	30	44	63	90	128	182
	1	20	30	44	63	90	128	182
	1	20	30	44	63	90	128	182
PCG	2	40	80	160	320	640	1280	98
	4	40	80	31	82	640	1280	2560
	8	22	80	29	28	33	65	143
	16	nac	16	160	47	40	52	71
GMRES	1	20	45	80	147	303	624	1192
	1	20	45	80	147	303	624	1192
	1	20	45	80	147	303	624	1192
	1	20	45	80	147	303	624	1192
PGMRES	2	4	4	4	6	5	5	8
	4	5	5	6	7	10	11	12
	8	7	8	10	12	11	13	16
	16	nac	11	11	12	15	17	20

Table 5: Number of iterations for CG and GMRES with  $P_{BRAS,n}^{(\nu)}(A_n)$ , with overlap  $o = 5$ .

<b>Method</b>	$\nu$	$n = 40$	$n = 80$	$n = 160$	$n = 320$	$n = 640$	$n = 1280$	$n = 2560$
CG	1	20	30	44	63	90	128	182
	1	20	30	44	63	90	128	182
	1	20	30	44	63	90	128	182
	1	20	30	44	63	90	128	182
PCG	2	40	80	160	320	640	1280	2560
	4	33	80	160	46	640	1280	2560
	8	nac	26	160	30	37	35	84
	16	nac	nac	16	320	57	41	56
GMRES	1	20	45	80	147	303	624	1192
	1	20	45	80	147	303	624	1192
	1	20	45	80	147	303	624	1192
	1	20	45	80	147	303	624	1192
PGMRES	2	3	4	4	4	6	5	5
	4	5	5	5	6	7	11	12
	8	nac	8	7	8	13	12	14
	16	nac	nac	12	11	12	15	18

Table 6: Number of iterations for CG and GMRES with  $P_{BRAS,n}^{(\nu)}(A_n)$ , with overlap  $o = 10$ .

<b>Method</b>	$\nu$	$n = 40$	$n = 80$	$n = 160$	$n = 320$	$n = 640$	$n = 1280$	$n = 2560$
CG	1	20	30	44	63	90	128	182
	1	20	30	44	63	90	128	182
	1	20	30	44	63	90	128	182
	1	20	30	44	63	90	128	182
PCG	2	nac	9	160	320	640	1280	2560
	4	nac	nac	160	320	640	1280	2560
	8	nac	nac	nac	320	640	29	34
	16	nac	nac	nac	nac	640	1280	41
GMRES	1	20	45	80	147	303	624	1192
	1	20	45	80	147	303	624	1192
	1	20	45	80	147	303	624	1192
	1	20	45	80	147	303	624	1192
PGMRES	2	nac	3	3	4	4	4	7
	4	nac	nac	5	5	8	8	9
	8	nac	nac	nac	8	8	9	11
	16	nac	nac	nac	nac	11	12	14

Table 7: Number of iterations for CG and GMRES with  $P_{BRAS,n}^{(\nu)}(A_n)$ , for various  $n$  and  $\nu$ , overlap  $o = 30$ .

<b>Method</b>	$\nu$	$n = 40$	$n = 80$	$n = 160$	$n = 320$	$n = 640$	$n = 1280$	$n = 2560$
CG	1	20	30	44	63	90	128	182
	1	20	30	44	63	90	128	182
	1	20	30	44	63	90	128	182
	1	20	30	44	63	90	128	182
PCG	2	36	32	66	320	640	236	113
	4	40	80	160	320	640	1280	2560
	8	40	80	160	320	640	1280	2560
	16	40	80	160	320	640	1280	2560
GMRES	1	20	45	80	147	303	624	1192
	1	20	45	80	147	303	624	1192
	1	20	45	80	147	303	624	1192
	1	20	45	80	147	303	624	1192
PGMRES	2	4	5	7	5	5	8	9
	4	7	10	8	11	9	14	17
	8	10	13	14	16	16	19	17
	16	15	15	17	19	21	22	25

Table 8: Number of iterations for CG and GMRES with  $P_{BGS,n}^{(\nu)}(A_n)$ , with overlap  $o = 0$ .

<b>Method</b>	$\nu$	$n = 40$	$n = 80$	$n = 160$	$n = 320$	$n = 640$	$n = 1280$	$n = 2560$
CG	1	20	30	44	63	90	128	182
	1	20	30	44	63	90	128	182
	1	20	30	44	63	90	128	182
	1	20	30	44	63	90	128	182
PCG	2	40	80	160	320	53	37	58
	4	40	80	160	320	640	1280	2560
	8	40	80	160	320	640	1280	2560
	16	nac	80	160	320	640	1280	2560
GMRES	1	20	45	80	147	303	624	1192
	1	20	45	80	147	303	624	1192
	1	20	45	80	147	303	624	1192
	1	nac	45	80	147	303	624	1192
PGMRES	2	3	3	4	4	4	4	6
	4	4	5	7	7	7	8	8
	8	5	7	8	9	11	12	14
	16	nac	8	11	14	15	15	17

Table 9: Number of iterations for CG and GMRES with  $P_{BMS,n}^{(\nu)}(A_n)$ , with overlap  $o = 5$ .

<b>Method</b>	$\nu$	$n = 40$	$n = 80$	$n = 160$	$n = 320$	$n = 640$	$n = 1280$	$n = 2560$
CG	1	20	30	44	63	90	128	182
	1	20	30	44	63	90	128	182
	1	20	30	44	63	90	128	182
	1	20	30	44	63	90	128	182
PCG	2	13	80	160	320	640	52	32
	4	13	80	160	320	640	1280	2560
	8	nac	80	160	320	640	1280	2560
	16	nac	nac	160	320	640	1280	2560
GMRES	1	20	45	80	147	303	624	1192
	1	20	45	80	147	303	624	1192
	1	20	45	80	147	303	624	1192
	1	20	45	80	147	303	624	1192
PGMRES	2	3	3	3	4	4	4	5
	4	3	4	5	7	7	7	9
	8	nac	5	7	9	9	11	12
	16	nac	nac	8	11	14	15	15

Table 10: Number of iterations for CG and GMRES with  $P_{BMS,n}^{(\nu)}(A_n)$ , with overlap  $o = 10$ .

<b>Method</b>	$\nu$	$n = 40$	$n = 80$	$n = 160$	$n = 320$	$n = 640$	$n = 1280$	$n = 2560$
CG	1	20	30	44	63	90	128	182
	1	20	30	44	63	90	128	182
	1	20	30	44	63	90	128	182
	1	20	30	44	63	90	128	182
PCG	2	nac	6	160	320	640	1280	144
	4	nac	nac	160	320	640	1280	2560
	8	nac	nac	nac	320	640	1280	2560
	16	nac	nac	nac	nac	640	1280	2560
GMRES	1	20	45	80	147	303	624	1192
	1	20	45	80	147	303	624	1192
	1	20	45	80	147	303	624	1192
	1	20	45	80	147	303	624	1192
PGMRES	2	nac	2	3	3	3	4	4
	4	nac	nac	4	5	5	6	9
	8	nac	nac	nac	6	8	9	9
	16	nac	nac	nac	nac	9	13	15

Table 11: Number of iterations for CG and GMRES with  $P_{BMS,n}^{(\nu)}(A_n)$ , with overlap  $o = 30$ .

<b>Method</b>	$\nu$	$n = 40$	$n = 80$	$n = 160$	$n = 320$	$n = 640$	$n = 1280$	$n = 2560$
CG	1	20	30	44	63	90	128	182
	1	20	30	44	63	90	128	182
	1	20	30	44	63	90	128	182
	1	20	30	44	63	90	128	182
PCG	2	40	80	160	320	640	1280	2560
	4	40	80	160	320	640	1280	2560
	8	40	80	160	320	640	1280	2560
	16	nac	80	160	320	640	1280	2560
GMRES	1	20	45	80	147	303	624	1192
	1	20	45	80	147	303	624	1192
	1	20	45	80	147	303	624	1192
	1	20	45	80	147	303	624	1192
PGMRES	2	3	3	5	4	4	5	6
	4	6	5	6	7	7	8	8
	8	7	8	10	9	11	13	15
	16	nac	10	14	15	16	16	17

Table 12: Number of iterations for CG and GMRES with  $P_{BRMS,n}^{(\nu)}(A_n)$ , with overlap  $o = 5$ .

<b>Method</b>	$\nu$	$n = 40$	$n = 80$	$n = 160$	$n = 320$	$n = 640$	$n = 1280$	$n = 2560$
CG	1	20	30	44	63	90	128	182
	1	20	30	44	63	90	128	182
	1	20	30	44	63	90	128	182
	1	20	30	44	63	90	128	182
PCG	2	40	80	160	320	640	1280	2560
	4	40	80	160	320	640	1280	2560
	8	nac	80	160	320	640	1280	2560
	16	nac	nac	160	320	640	1280	2560
GMRES	1	20	45	80	147	303	624	1192
	1	20	45	80	147	303	624	1192
	1	20	45	80	147	303	624	1192
	1	20	45	80	147	303	624	1192
PGMRES	2	3	3	4	5	4	4	5
	4	4	5	5	6	8	7	9
	8	nac	7	8	10	9	12	13
	16	nac	nac	10	14	15	16	16

Table 13: Number of iterations for CG and GMRES with  $P_{BRMS,n}^{(\nu)}(A_n)$ , with overlap  $o = 10$ .

<b>Method</b>	$\nu$	$n = 40$	$n = 80$	$n = 160$	$n = 320$	$n = 640$	$n = 1280$	$n = 2560$
CG	1	20	30	44	63	90	128	182
	1	20	30	44	63	90	128	182
	1	20	30	44	63	90	128	182
	1	20	30	44	63	90	128	182
PCG	2	nac	25	160	320	640	1280	2560
	4	nac	nac	160	320	640	1280	2560
	8	nac	nac	nac	320	640	1280	2560
	16	nac	nac	nac	nac	640	1280	2560
GMRES	1	20	45	80	147	303	624	1192
	1	20	45	80	147	303	624	1192
	1	20	45	80	147	303	624	1192
	1	20	45	80	147	303	624	1192
PGMRES	2	nac	3	3	3	5	4	4
	4	nac	nac	5	5	7	6	7
	8	nac	nac	nac	8	9	9	11
	16	nac	nac	nac	nac	12	15	16

Table 14: Number of iterations for CG and GMRES with  $P_{BRMS,n}^{(\nu)}(A_n)$ , with overlap  $o = 30$ .

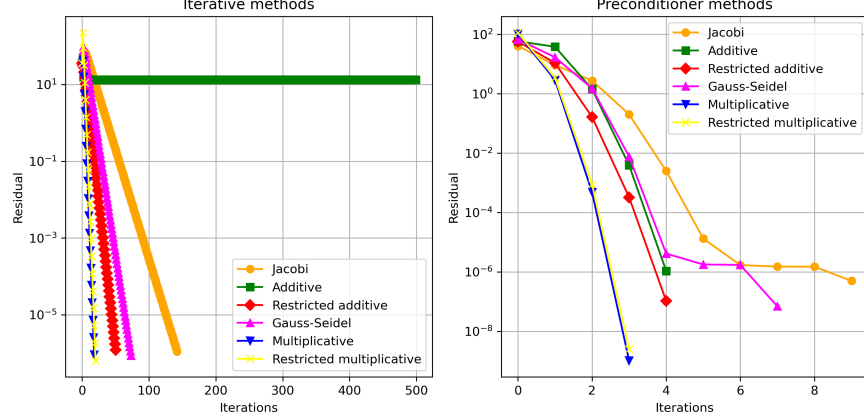


Figure 2: Comparison of iterative and preconditioner methods using GMRES. The left plot shows the residuals for standard iterative methods, while the right plot shows residuals for preconditioned methods. The simulation is performed with matrix size  $n = 1280$ , number of subdomains  $\nu = 2$ , and overlap  $o = 30$ .

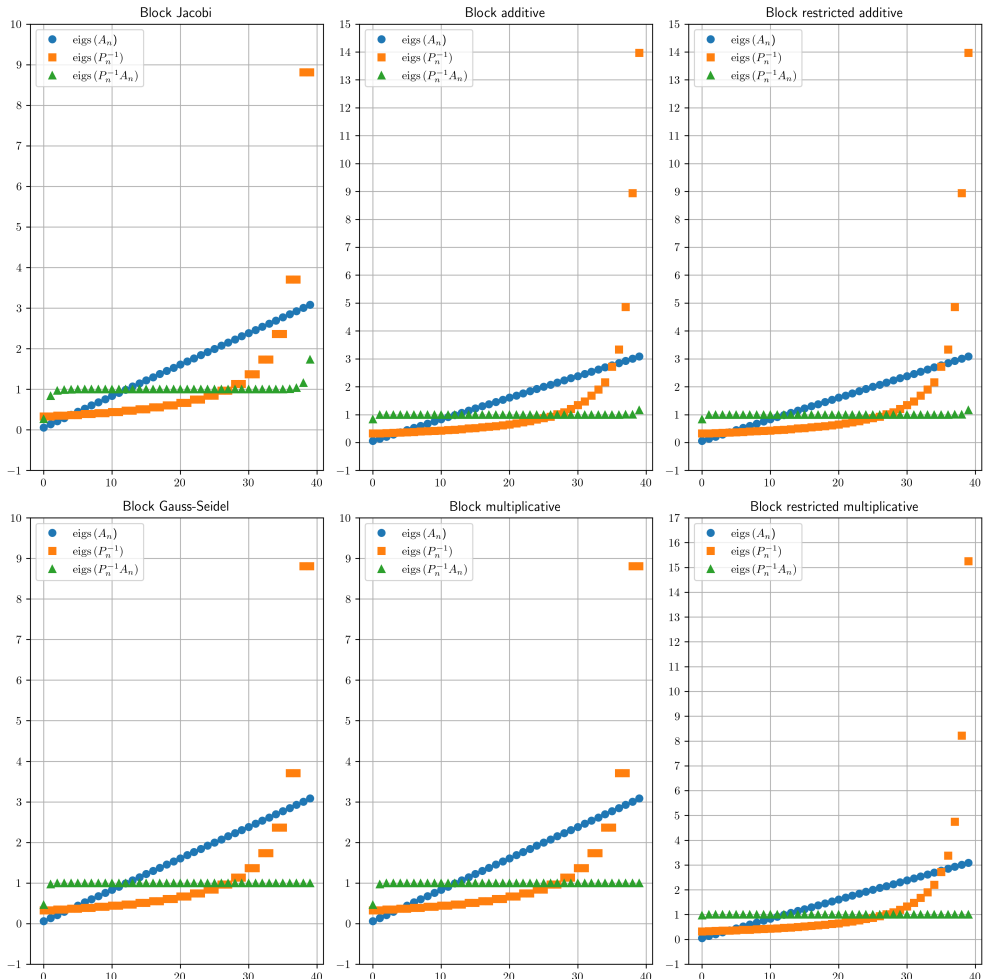


Figure 3: Comparison of eigenvalues for different block methods with matrix size  $n = 40$ , number of subdomains  $\nu = 2$ , and overlap  $o = 10$ . The markers represent the eigenvalues of  $A_n$ ,  $P_n^{-1}$ , and  $P_n^{-1} A_n$  for each method.

**Remark 6.1.** Both multiplicative and restricted additive Schwarz preconditioners are, in general, not Hermitian. This point is crucial when selecting an iterative solver: GMRES can be applied directly, whereas CG requires an HPD preconditioner.

**Example 6.2** (The finite difference discretization  $s = 1$ ). Consider the second-order differential problem

$$\begin{cases} -\left(a(x)u'(x)\right)' = f(x), & x \in (0, 1), \\ u(0) = \alpha, & u(1) = \beta, \end{cases} \quad (24)$$

where  $a \in C([0, 1])$  and  $f$  is a given function. To guarantee well-posedness, one typically imposes additional assumptions, for example

$$f \in L^2(0, 1), \quad a \in C^1([0, 1]), \quad a(x) > 0, \text{ for all } x \in [0, 1].$$

Equation (24) defines an elliptic boundary-value problem. For the purposes of GLT analysis, it is sufficient to assume the weaker condition  $a \in C([0, 1])$ , since no further regularity is necessary.

We discretize (24) using the classical second-order central finite difference scheme on a uniform grid. When  $a(x)$  is constant (for example  $a(x) = 1, \forall x$ ), this reduces to the familiar  $(-1, 2, -1)$  stencil. Given a discretization parameter  $n \in \mathbb{N}$ , define

$$h = \frac{1}{n+1}, \quad x_j = jh, \quad j = 0, 1, \dots, n+1.$$

For  $j = 1, \dots, n$ , we approximate  $-(a(x)u'(x))'$  at  $x = x_j$  by the classical second-order central FD formula:

$$\begin{aligned} -(a(x)u'(x_j))' &\approx -\frac{a(x_{j+\frac{1}{2}})u'(x_{j+\frac{1}{2}}) - a(x_{j-\frac{1}{2}})u'(x_{j-\frac{1}{2}})}{h} \\ &\approx -\frac{a(x_{j+\frac{1}{2}})u_{j+1} - (a(x_{j+\frac{1}{2}}) + a(x_{j-\frac{1}{2}}))u_j + a(x_{j-\frac{1}{2}})u_{j-1}}{h^2}, \end{aligned} \quad (25)$$

where  $u_j = u(x_j)$ . This means that the nodal values of the solution  $u$  satisfy the following linear system:

$$-a(x_{j+\frac{1}{2}})u_{j+1} + (a(x_{j+\frac{1}{2}}) - a(x_{j-\frac{1}{2}}))u_j + a(x_{j-\frac{1}{2}})u_{j-1} = h^2 f(x_j), \quad j = 1, \dots, n. \quad (26)$$

The matrix of the linear system (26) is the  $n \times n$  tridiagonal symmetric matrix given by

$$A_n = \begin{bmatrix} a_{1/2} + a_{3/2} & -a_{3/2} & 0 & \cdots & 0 \\ -a_{3/2} & a_{3/2} + a_{5/2} & -a_{5/2} & \ddots & \vdots \\ 0 & -a_{5/2} & a_{5/2} + a_{7/2} & \ddots & 0 \\ \vdots & \ddots & \ddots & \ddots & -a_{n-1/2} \\ 0 & \cdots & 0 & -a_{n-1/2} & a_{n+1/2} + a_{n-1/2} \end{bmatrix},$$

where  $a_{j+\frac{1}{2}} = a(x_j + \frac{h}{2})$ ,  $j = 1, \dots, n$ .

Within the GLT framework, it is well established that the matrix sequence  $\{A_n\}_n$  admits the symbol

$$\{A_n\}_n \sim_{\text{GLT}} a(x) (2 - 2 \cos \theta).$$

Building upon this characterization, our analysis shows that the same GLT symbol is inherited by all classical block preconditioner sequences  $\{P_{\star,n}^{(\nu)}\}_n$ , namely,

$$\{P_{\star,n}^{(\nu)}\}_n \sim_{\text{GLT}} a(x) (2 - 2 \cos \theta).$$

In the non-overlapping setting, Theorem (5.1) establishes the validity of this result for

$$\star \in \{\text{BJ, BAS, BGS, BMS}\}.$$

This theoretical prediction is fully corroborated by the numerical experiments for the constant coefficient case  $a(x) = 1$ , see Figures 4–7, and for the variable coefficient case  $a(x) = 1 + x^2$ , see Figures 10–13.

For the overlapping additive, Theorem (5.2) applies, yielding

$$\star \in \{\text{BAS}\}.$$

Once again, the predicted GLT behavior is in excellent agreement with the observed spectral distributions for  $a(x) = 1$ , see Figure 5, and for  $a(x) = 1 + x^2$ , see Figure 11.

In the overlapping multiplicative case, Theorem (5.3) ensures the preservation of the GLT symbol for

$$\star \in \{\text{BMS}\}.$$

The numerical evidence confirms this result for the constant coefficient case  $a(x) = 1$ , see Figure 8, and for the variable coefficient case  $a(x) = 1 + x^2$ , see Figure 14.

Finally, concerning the restricted overlapping variants, Theorem (5.4) applies, covering

$$\star \in \{\text{BRAS, BRMS}\}.$$

The corresponding numerical experiments once more validate the theoretical analysis for  $a(x) = 1$ , see Figures 6–9, and for  $a(x) = 1 + x^2$ , see Figures 12–15.

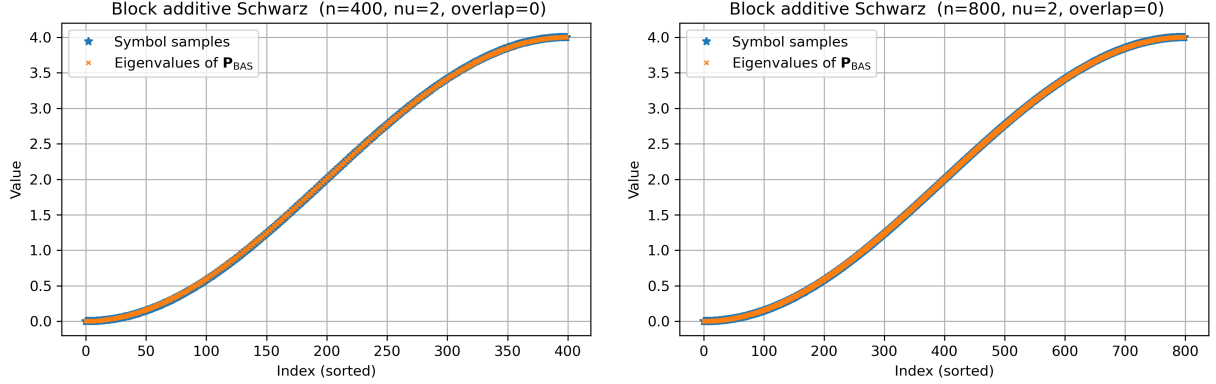


Figure 4: Comparison between the GLT symbol  $(2 - 2 \cos \theta)$  and the eigenvalues of the block additive Schwarz preconditioner  $P_{\text{BAS},n}^{(\nu)}$  without overlap. Left:  $n = 400$ ,  $\nu = 2$ . Right:  $n = 800$ ,  $\nu = 2$ .

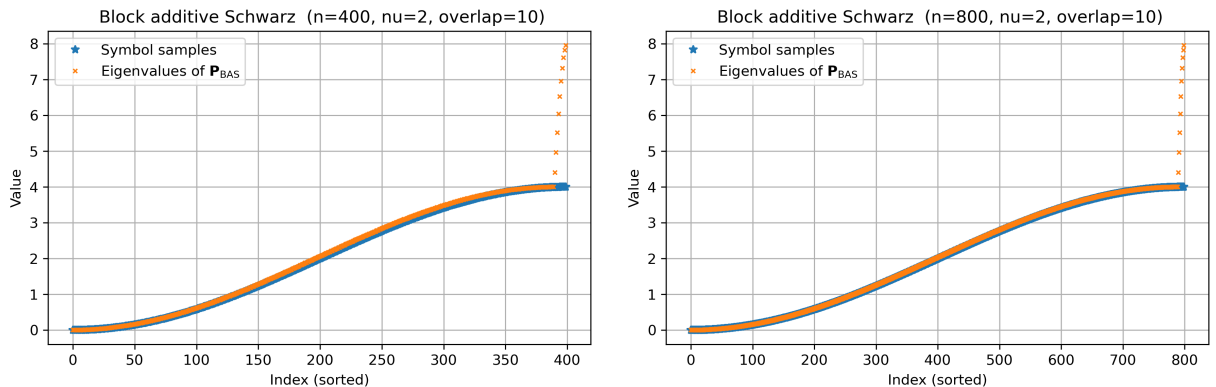


Figure 5: Comparison between the GLT symbol  $(2 - 2 \cos \theta)$  and the eigenvalues of the block additive Schwarz preconditioner  $P_{\text{BAS},n}^{(\nu)}$  with overlap  $o = 10$ . Left:  $n = 400$ ,  $\nu = 2$ . Right:  $n = 800$ ,  $\nu = 2$ .

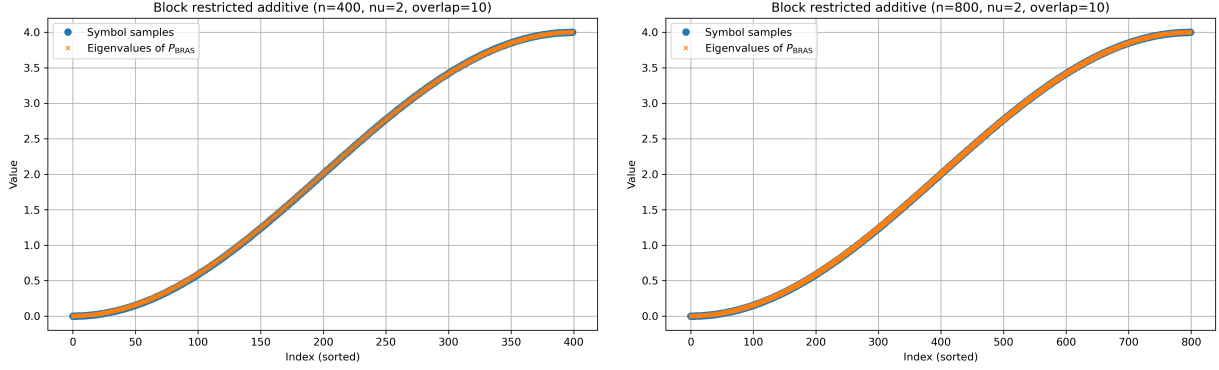


Figure 6: Comparison between the GLT symbol ( $2 - 2 \cos \theta$ ) and the eigenvalues of the block restricted additive Schwarz preconditioner  $P_{\text{BRAS},n}^{(\nu)}$  with overlap  $o = 10$ . Left:  $n = 400, \nu = 2$ . Right:  $n = 800, \nu = 2$ .

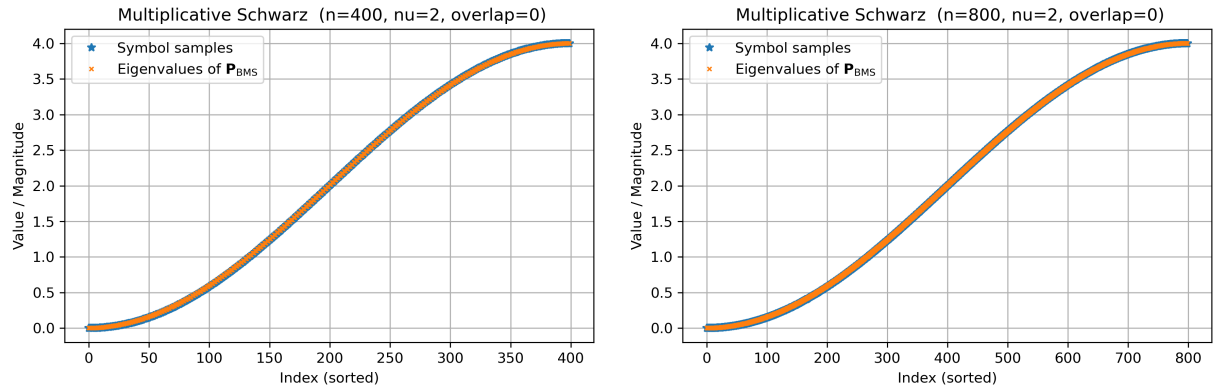


Figure 7: Comparison between the GLT symbol ( $2 - 2 \cos \theta$ ) and the eigenvalues of the block multiplicative Schwarz preconditioner  $P_{\text{BMS},n}^{(\nu)}$  without overlap. Left:  $n = 400, \nu = 2$ . Right:  $n = 800, \nu = 2$ .

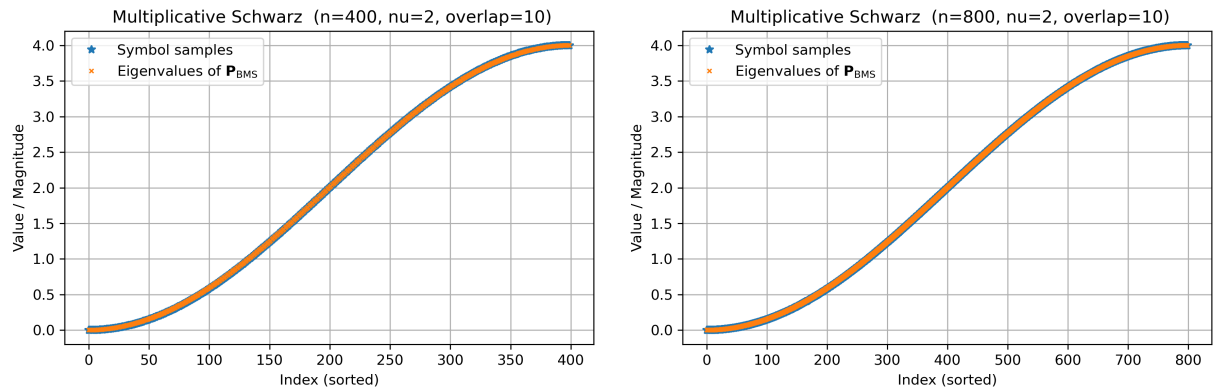


Figure 8: Comparison between the GLT symbol ( $2 - 2 \cos \theta$ ) and the eigenvalues of the block multiplicative Schwarz preconditioner  $P_{\text{BMS},n}^{(\nu)}$ , with overlap  $o = 10$ . Left:  $n = 400, \nu = 2$ . Right:  $n = 800, \nu = 2$ .

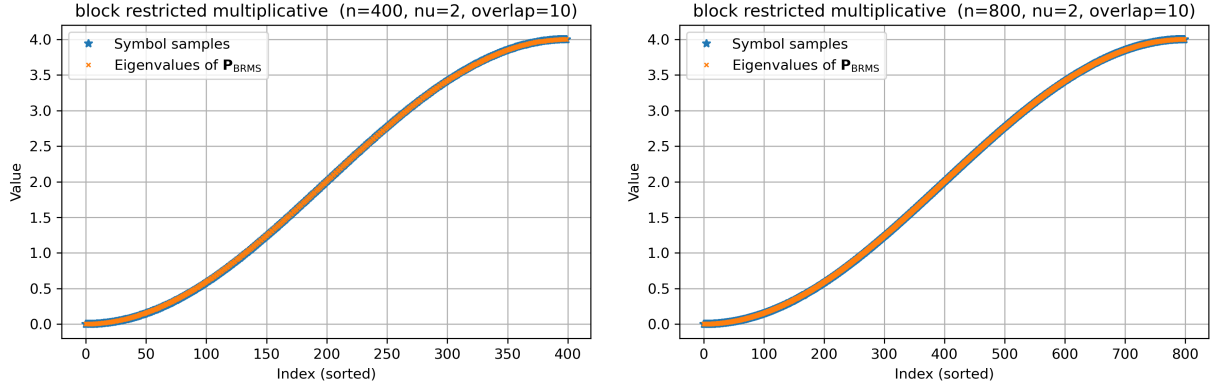


Figure 9: Comparison between the GLT symbol  $(2 - 2 \cos \theta)$  and the eigenvalues of block restricted multiplicative Schwarz preconditioner  $P_{BRMS,n}^{(\nu)}$  with overlap  $o = 10$ . Left:  $n = 400$ ,  $\nu = 2$ . Right:  $n = 800$ ,  $\nu = 2$ .

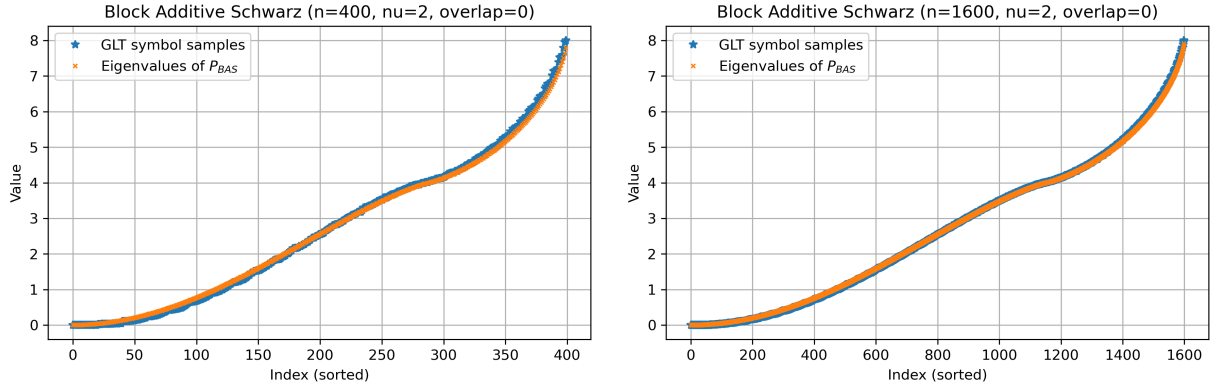


Figure 10: Comparison between the GLT symbol  $(1 + x^2)(2 - 2 \cos \theta)$  and the eigenvalues of the block additive Schwarz preconditioner  $P_{BAS,n}^{(\nu)}$  without overlap. Left:  $n = 400$ ,  $\nu = 2$ . Right:  $n = 1600$ ,  $\nu = 2$ .

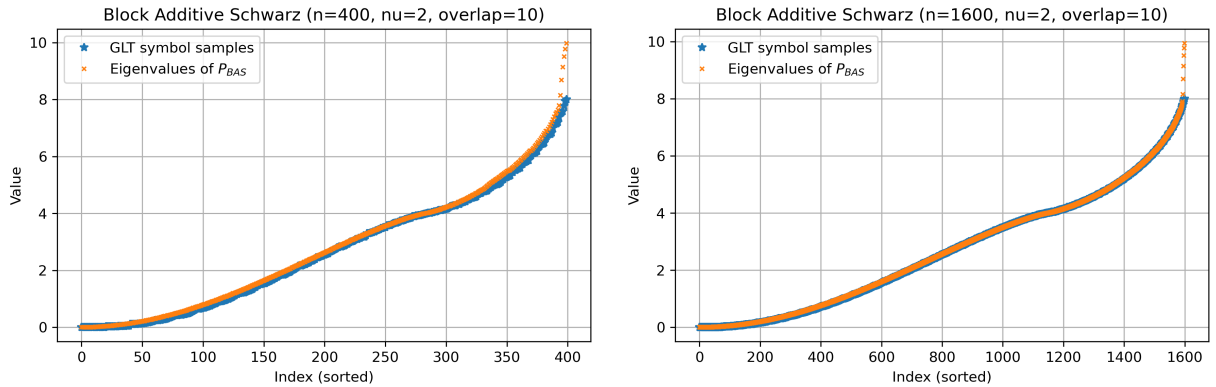


Figure 11: Comparison between the GLT symbol  $(1 + x^2)(2 - 2 \cos \theta)$  and the eigenvalues of the block additive Schwarz preconditioner  $P_{BAS,n}^{(\nu)}$  with overlap  $o = 10$ . Left:  $n = 400$ ,  $\nu = 2$ . Right:  $n = 1600$ ,  $\nu = 2$ .

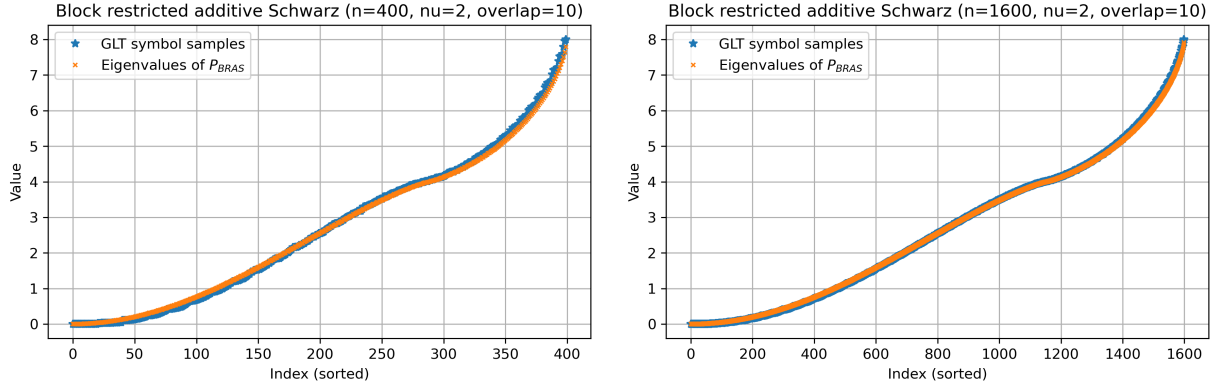


Figure 12: Comparison between the GLT symbol  $(1 + x^2)(2 - 2 \cos \theta)$  and the eigenvalues of the block restricted additive Schwarz preconditioner  $P_{BRAS,n}^{(\nu)}$  with overlap  $o = 10$ . Left:  $n = 400$ ,  $\nu = 2$ . Right:  $n = 1600$ ,  $\nu = 2$ .

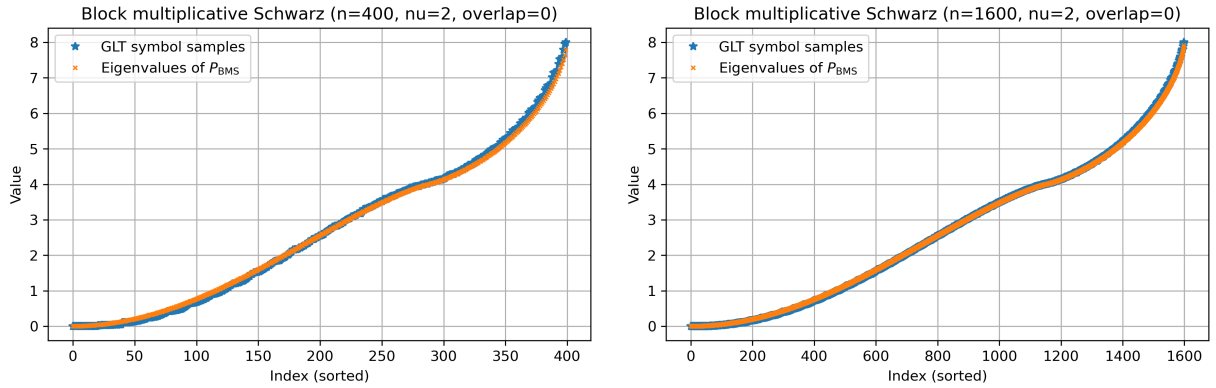


Figure 13: Comparison between the GLT symbol  $(1 + x^2)(2 - 2 \cos \theta)$  and the eigenvalues of the block multiplicative Schwarz preconditioner  $P_{BMS,n}^{(\nu)}$  without overlap. Left:  $n = 400$ ,  $\nu = 2$ . Right:  $n = 1600$ ,  $\nu = 2$ .

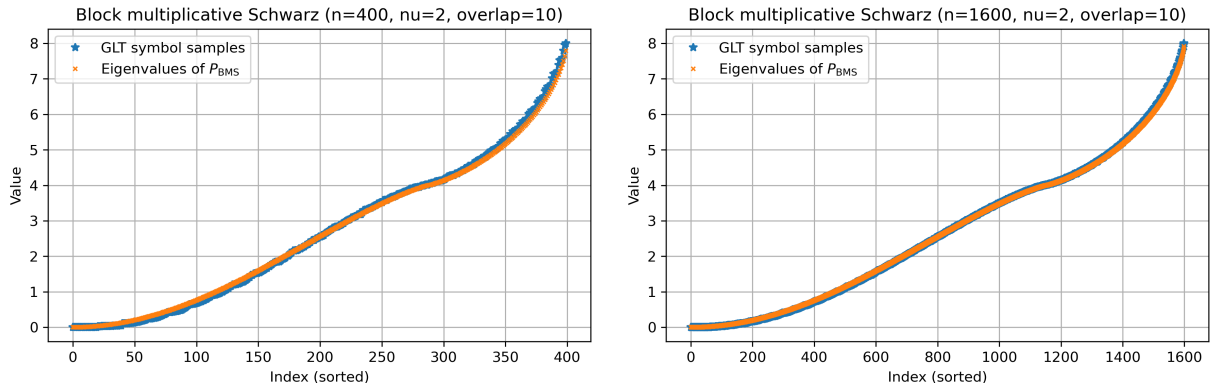


Figure 14: Comparison between the GLT symbol  $(1 + x^2)(2 - 2 \cos \theta)$  and the eigenvalues of the block multiplicative Schwarz preconditioner  $P_{BMS,n}^{(\nu)}$  with overlap  $o = 10$ . Left:  $n = 400$ ,  $\nu = 2$ . Right:  $n = 1600$ ,  $\nu = 2$ .

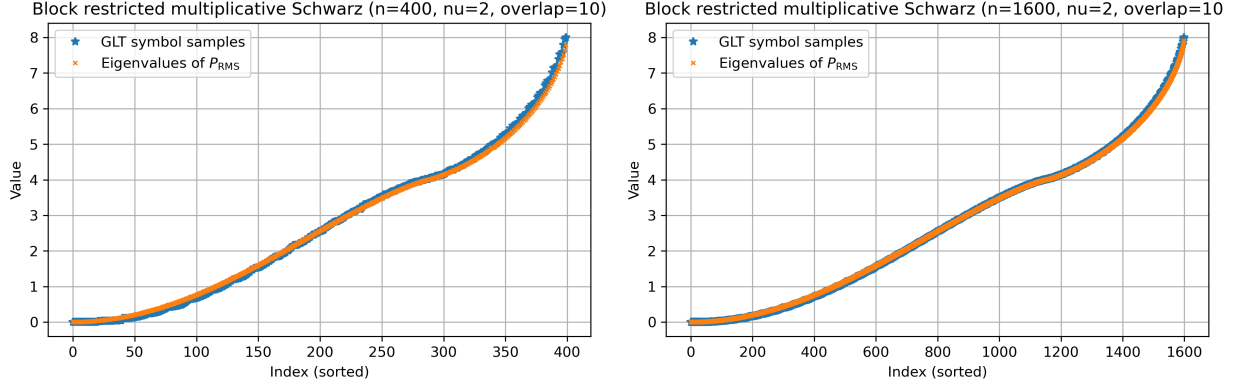


Figure 15: Comparison between the GLT symbol  $(1 + x^2)(2 - 2 \cos \theta)$  and the eigenvalues of the block restricted multiplicative Schwarz preconditioner  $P_{\text{BRMS},n}^{(\nu)}(A_n)$  with overlap  $o = 10$ . Left:  $n = 400$ ,  $\nu = 2$ . Right:  $n = 1600$ ,  $\nu = 2$ .

Tables 15–17 report the clustering of eigenvalues of  $\left\{ (P_{\star,n}^{(\nu)}(A_n))^{-1} A_n \right\}_n$  around 1, measured by

$$\frac{\#\{j : |\lambda_j((P_{\star,n}^{(\nu)}(A_n))^{-1} A_n) - 1| > \varepsilon\}}{n},$$

for  $\star \in \{\text{BAS, BMS}\}$ . Tables 16–18 report the same clustering without normalization

$$\#\{j : |\lambda_j((P_{\star,n}^{(\nu)}(A_n))^{-1} A_n) - 1| > \varepsilon\},$$

for  $\star \in \{\text{BRAS, BRMS}\}$ , considering various values of  $n$ ,  $\nu$ , and overlap  $o = 5$ .

$\nu / \varepsilon$	$n = 40$	$n = 80$	$n = 160$	$n = 320$	$n = 640$	$n = 1280$	$n = 2560$
$\nu = 2 / \varepsilon = 1.0e^{-01}$	0.30	0.15	0.07	0.04	0.02	0.01	0.00
$\nu = 2 / \varepsilon = 5.0e^{-02}$	0.30	0.15	0.07	0.04	0.02	0.01	0.00
$\nu = 2 / \varepsilon = 2.5e^{-02}$	0.30	0.15	0.07	0.04	0.02	0.01	0.00
$\nu = 4 / \varepsilon = 1.0e^{-01}$	0.80	0.45	0.23	0.11	0.06	0.03	0.01
$\nu = 4 / \varepsilon = 5.0e^{-02}$	0.80	0.45	0.23	0.11	0.06	0.03	0.01
$\nu = 4 / \varepsilon = 2.5e^{-02}$	0.80	0.45	0.23	0.11	0.06	0.03	0.01
$\nu = 8 / \varepsilon = 1.0e^{-01}$	1.00	0.89	0.53	0.26	0.13	0.07	0.03
$\nu = 8 / \varepsilon = 5.0e^{-02}$	1.00	0.90	0.53	0.26	0.13	0.07	0.03
$\nu = 8 / \varepsilon = 2.5e^{-02}$	1.00	0.90	0.53	0.26	0.13	0.07	0.03

Table 15: Clustering of the eigenvalues of  $\left\{ (P_{\text{BAS},n}^{(\nu)}(A_n))^{-1} A_n \right\}_n$  around 1, measured by  $\#\{j : |\lambda_j((P_{\text{BAS},n}^{(\nu)}(A_n))^{-1} A_n) - 1| > \varepsilon\}$ , for various  $n$  and  $\nu$  with overlap  $o = 5$ .

$n$	$\nu / \varepsilon$	$n = 40$	$n = 80$	$n = 160$	$n = 320$	$n = 640$	$n = 1280$	$n = 2560$
$\nu = 2 / \varepsilon = 1.0e^{-01}$	12	12	12	12	12	12	12	12
$\nu = 2 / \varepsilon = 5.0e^{-02}$	12	12	12	12	12	12	12	12
$\nu = 2 / \varepsilon = 2.5e^{-02}$	12	12	12	12	12	12	12	12
$\nu = 4 / \varepsilon = 1.0e^{-01}$	32	36	36	36	36	36	36	36
$\nu = 4 / \varepsilon = 5.0e^{-02}$	32	36	36	36	36	36	36	36
$\nu = 4 / \varepsilon = 2.5e^{-02}$	32	36	36	36	36	36	36	36
$\nu = 8 / \varepsilon = 1.0e^{-01}$	40	71	84	84	84	84	84	84
$\nu = 8 / \varepsilon = 5.0e^{-02}$	40	72	84	84	84	84	84	84
$\nu = 8 / \varepsilon = 2.5e^{-02}$	40	72	84	84	84	84	84	84

Table 16: Clustering of the eigenvalues of  $\left\{ (P_{\text{BAS},n}^{(\nu)}(A_n))^{-1} A_n \right\}_n$  around 1, measured by  $\#\{j : |\lambda_j((P_{\text{BAS},n}^{(\nu)}(A_n))^{-1} A_n) - 1| > \varepsilon\}$ , for various values of  $n$  and  $\nu$  with overlap  $o = 5$ .

$\nu / \varepsilon$	$n = 40$	$n = 80$	$n = 160$	$n = 320$	$n = 640$	$n = 1280$	$n = 2560$
$\nu = 2/\varepsilon = 1.0e^{-01}$	0.03	0.01	0.01	0.00	0.00	0.00	0.00
$\nu = 2/\varepsilon = 5.0e^{-02}$	0.03	0.01	0.01	0.00	0.00	0.00	0.00
$\nu = 2/\varepsilon = 2.5e^{-02}$	0.03	0.01	0.01	0.00	0.00	0.00	0.00
$\nu = 4/\varepsilon = 1.0e^{-01}$	0.03	0.04	0.02	0.01	0.00	0.00	0.00
$\nu = 4/\varepsilon = 5.0e^{-02}$	0.03	0.04	0.02	0.01	0.00	0.00	0.00
$\nu = 4/\varepsilon = 2.5e^{-02}$	0.05	0.04	0.02	0.01	0.00	0.00	0.00
$\nu = 8/\varepsilon = 1.0e^{-01}$	0.03	0.04	0.04	0.02	0.01	0.01	0.00
$\nu = 8/\varepsilon = 5.0e^{-02}$	0.05	0.04	0.04	0.02	0.01	0.01	0.00
$\nu = 8/\varepsilon = 2.5e^{-02}$	0.05	0.04	0.04	0.02	0.01	0.01	0.00

Table 17: Clustering of the eigenvalues of  $\left\{ (P_{\text{BMS},n}^{(\nu)}(A_n))^{-1} A_n \right\}_n$  around 1, measured by  $\frac{\#\{j : |\lambda_j((P_{\text{BMS},n}^{(\nu)}(A_n))^{-1} A_n) - 1| > \varepsilon\}}{n}$ , for various values of  $n$  and  $\nu$  with overlap  $o = 5$ .

$\nu / \varepsilon$	$n = 40$	$n = 80$	$n = 160$	$n = 320$	$n = 640$	$n = 1280$	$n = 2560$
$\nu = 2/\varepsilon = 1.0e^{-01}$	1	1	1	1	1	1	1
$\nu = 2/\varepsilon = 5.0e^{-02}$	1	1	1	1	1	1	1
$\nu = 2/\varepsilon = 2.5e^{-02}$	1	1	1	1	1	1	1
$\nu = 4/\varepsilon = 1.0e^{-01}$	1	3	3	3	3	3	3
$\nu = 4/\varepsilon = 5.0e^{-02}$	1	3	3	3	3	3	3
$\nu = 4/\varepsilon = 2.5e^{-02}$	2	3	3	3	3	3	3
$\nu = 8/\varepsilon = 1.0e^{-01}$	1	3	6	7	7	7	7
$\nu = 8/\varepsilon = 5.0e^{-02}$	2	3	7	7	7	7	7
$\nu = 8/\varepsilon = 2.5e^{-02}$	2	3	7	7	7	7	7

Table 18: Clustering of the eigenvalues of  $\left\{ (P_{\text{BMS},n}^{(\nu)}(A_n))^{-1} A_n \right\}_n$  around 1, measured by  $\#\{j : |\lambda_j((P_{\text{BMS},n}^{(\nu)}(A_n))^{-1} A_n) - 1| > \varepsilon\}$ , for various values of  $n$  and  $\nu$  with overlap  $o = 5$ .

The number  $s$  in item (A) is given by  $s = 1$ , we follow the program in item (B). The results are collected in Tables (19)–(22)

Method	$\nu$	$n = 40$	$n = 80$	$n = 160$	$n = 320$	$n = 640$	$n = 1280$	$n = 2560$
CG	1	40	80	160	320	640	1280	2560
	1	40	80	160	320	640	1280	2560
	1	40	80	160	320	640	1280	2560
	1	40	80	160	320	640	1280	2560
PCG	2	4	4	4	4	4	4	4
	4	8	8	8	8	8	8	8
	8	10	14	16	16	16	17	17
	16	nac	15	22	28	32	33	33
GMRES	1	40	80	160	320	640	1280	2560
	1	40	80	160	320	640	1280	2560
	1	40	80	160	320	640	1280	2560
	1	40	80	160	320	640	1280	2560
PGMRES	2	4	4	4	4	4	4	4
	4	8	8	8	8	8	8	15
	8	15	14	16	23	16	21	17
	16	nac	17	34	60	120	140	125

Table 19: Number of iterations for CG and GMRES with  $P_{\text{BAS},n}^{(\nu)}(A_n)$ , with overlap  $o = 5$ .

<b>Method</b>	$\nu$	$n = 40$	$n = 80$	$n = 160$	$n = 320$	$n = 640$	$n = 1280$	$n = 2560$
CG	1	40	80	160	320	640	1280	2560
	1	40	80	160	320	640	1280	2560
	1	40	80	160	320	640	1280	2560
	1	40	80	160	320	640	1280	2560
PCG	2	40	80	160	320	640	1280	91
	4	40	80	160	320	640	105	39
	8	40	80	160	320	640	1280	152
	16	nac	80	160	320	640	1280	2560
GMRES	1	40	80	160	320	640	1280	2560
	1	40	80	160	320	640	1280	2560
	1	40	80	160	320	640	1280	2560
	1	40	80	160	320	640	1280	2560
PGMRES	2	2	2	2	2	2	2	4
	4	4	4	4	4	4	7	8
	8	5	8	8	8	8	16	9
	16	nac	12	16	16	16	17	21

Table 20: Number of iterations for CG and GMRES with  $P_{BMS,n}^{(\nu)}(A_n)$ , with overlap  $o = 5$ .

<b>Method</b>	$\nu$	$n = 40$	$n = 80$	$n = 160$	$n = 320$	$n = 640$	$n = 1280$	$n = 2560$
CG	1	40	80	160	320	640	1280	2560
	1	40	80	160	320	640	1280	2560
	1	40	80	160	320	640	1280	2560
	1	40	80	160	320	640	1280	2560
PCG	2	40	80	160	320	640	145	47
	4	40	80	160	124	79	60	56
	8	40	80	154	320	239	175	124
	16	nac	80	160	291	239	341	313
GMRES	1	40	80	160	320	640	1280	2560
	1	40	80	160	320	640	1280	2560
	1	40	80	160	320	640	1280	2560
	1	40	80	160	320	640	1280	2560
PGMRES	2	3	3	3	3	3	3	3
	4	7	7	7	7	7	7	14
	8	16	13	15	15	15	28	16
	16	nac	29	23	63	104	147	126

Table 21: Number of iterations for CG and GMRES with  $P_{BRAS,n}^{(\nu)}(A_n)$ , with overlap  $o = 5$ .

<b>Method</b>	$\nu$	$n = 40$	$n = 80$	$n = 160$	$n = 320$	$n = 640$	$n = 1280$	$n = 2560$
CG	1	40	80	160	320	640	1280	2560
	1	40	80	160	320	640	1280	2560
	1	40	80	160	320	640	1280	2560
	1	40	80	160	320	640	1280	2560
PCG	2	40	80	160	320	640	1280	2560
	4	40	80	160	320	640	1280	2560
	8	40	80	160	320	640	1280	2560
	16	nac	80	160	320	640	1280	2560
GMRES	1	40	80	160	320	640	1280	2560
	1	40	80	160	320	640	1280	2560
	1	40	80	160	320	640	1280	2560
	1	nac	80	160	320	640	1280	2560
PGMRES	2	2	2	2	2	2	2	4
	4	4	4	4	4	4	8	8
	8	10	8	8	8	10	15	9
	16	nac	17	16	16	18	17	30

Table 22: Number of iterations for CG and GMRES with  $P_{BRMS,n}^{(\nu)}(A_n)$ , with overlap  $o = 5$ .

**Example 6.3** (Finite element methods with  $s = 1$ ). Consider the one-dimensional elliptic boundary value problem

$$\begin{cases} -(a(x)u'(x))' = f(x), & x \in (0, 1), \\ u(0) = u(1) = 0. \end{cases} \quad (27)$$

We assume that the diffusion coefficient  $a : [0, 1] \rightarrow \mathbb{R}$  is continuous and uniformly positive, that is,  $a \in C([0, 1])$ ,  $a(x) > 0$  for all  $x \in [0, 1]$ , moreover, we assume that the source term satisfies  $f \in L^2(0, 1)$ .

The weak formulation of (27) reads as follows: find  $u \in H_0^1(0, 1)$  such that

$$\int_0^1 a(x) u'(x) v'(x) dx = \int_0^1 f(x) v(x) dx, \quad \forall v \in H_0^1(0, 1). \quad (28)$$

We now introduce a standard finite element discretization. Let  $n \in \mathbb{N}$  and set

$$h = \frac{1}{n+1}, \quad x_i = ih, \quad i = 0, \dots, n+1,$$

which defines a uniform partition of the interval  $[0, 1]$ ,  $0 = x_0 < x_1 < \dots < x_{n+1} = 1$ . We consider the classical linear finite element space

$$V_h = \{v \in H_0^1(0, 1) \mid v|_{[x_i, x_{i+1}]} \in \mathbb{P}_1, \quad i = 0, \dots, n\},$$

which consists of continuous, piecewise affine functions vanishing at the boundary. The space  $V_h$  admits the nodal basis  $V_h = \text{span}\{\varphi_1, \dots, \varphi_n\}$ , where  $\varphi_i$  is the standard hat function associated with the interior node  $x_i$ , defined by

$$\varphi_i(x) = \begin{cases} \frac{x - x_{i-1}}{x_i - x_{i-1}}, & x \in [x_{i-1}, x_i), \\ \frac{x_{i+1} - x}{x_{i+1} - x_i}, & x \in [x_i, x_{i+1}), \\ 0, & \text{otherwise,} \end{cases} \quad i = 1, \dots, n. \quad (29)$$

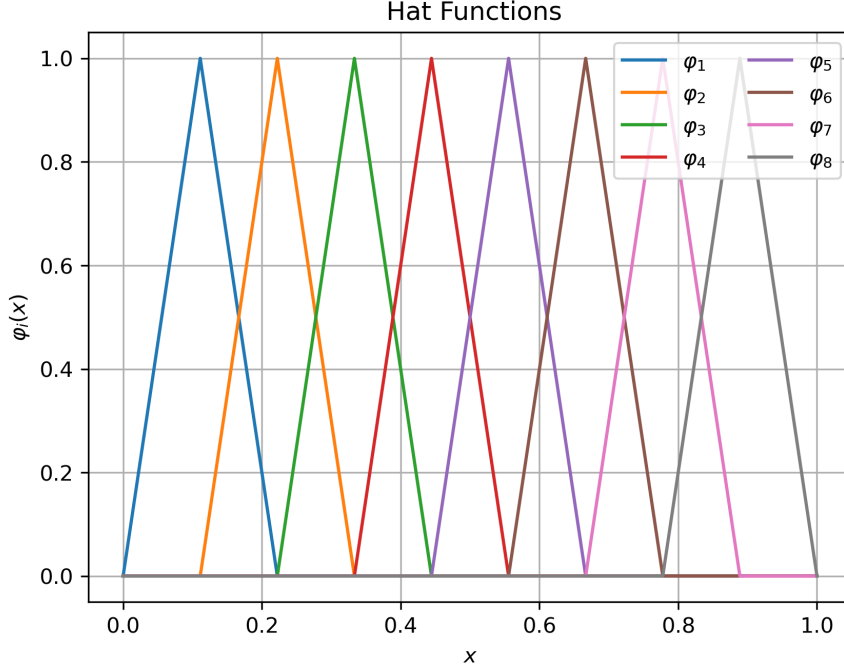
The finite element approximation of (27) consists in finding  $u_h \in V_h$  such that

$$\int_0^1 a(x) u'_h(x) v'(x) dx = \int_0^1 f(x) v(x) dx, \quad \forall v \in V_h. \quad (30)$$

Since  $\{\varphi_1, \dots, \varphi_n\}$  forms a basis of  $V_h$ , the discrete solution can be written as  $u_h(x) = \sum_{j=1}^n u_j \varphi_j(x)$ , where  $u = (u_1, \dots, u_n)^T \in \mathbb{R}^n$  is the vector of unknown coefficients. By linearity, the finite element problem reduces to solving the linear system

$$K_n u = f, \quad (31)$$

where the load vector  $f \in \mathbb{R}^n$  is given by  $f_i = \int_0^1 f(x) \varphi_i(x) dx$ ,  $i = 1, \dots, n$ , and the stiffness matrix  $K_n \in \mathbb{R}^{n \times n}$  has entries  $(K_n)_{ij} = \int_0^1 a(x) \varphi'_j(x) \varphi'_i(x) dx$ ,  $i, j = 1, \dots, n$ .

Figure 16: Graph of the hat-functions for  $n = 8$ .

Here, for each  $n \in \mathbb{N}$ , the following is also known in this case:

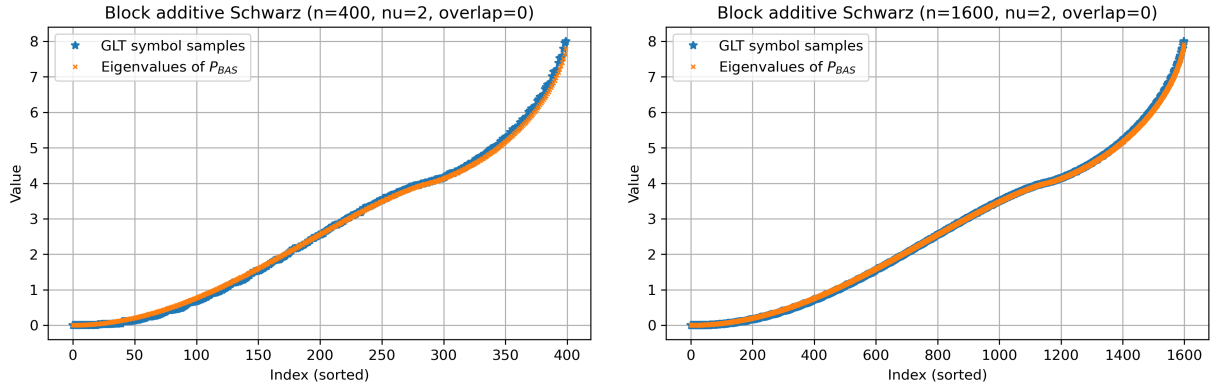
$$\left\{ \frac{1}{n+1} K_n \right\}_n \sim_{\text{GLT}} a(x) (2 - 2 \cos \theta). \quad (32)$$

$$\left\{ \frac{1}{n+1} K_n \right\}_n \sim_{\lambda, \sigma} a(x) (2 - 2 \cos \theta). \quad (33)$$

Therefore, by the case-by-case theoretical results established for each configuration (cf. Example (6.2)) and supported by the numerical evidence reported in the accompanying figures, any classical block preconditioner satisfies the predicted asymptotic behavior

$$\{P_{\star, n}^{(\nu)}\}_n \sim_{\text{GLT}} a(x) (2 - 2 \cos \theta), \quad \star \in \{\text{BJ, BAS, BRAS, BGS, BMS, BRMS}\}.$$

This conclusion is in full agreement with the numerical observations reported in Figures 17–22.

Figure 17: Comparison between the GLT symbol  $(1 + x^2)(2 - 2 \cos \theta)$  and the eigenvalues of the block additive Schwarz preconditioner  $P_{\text{BAS}, n}^{(\nu)}$  without overlap. Left:  $n = 400$ ,  $\nu = 2$ . Right:  $n = 1600$ ,  $\nu = 2$ .

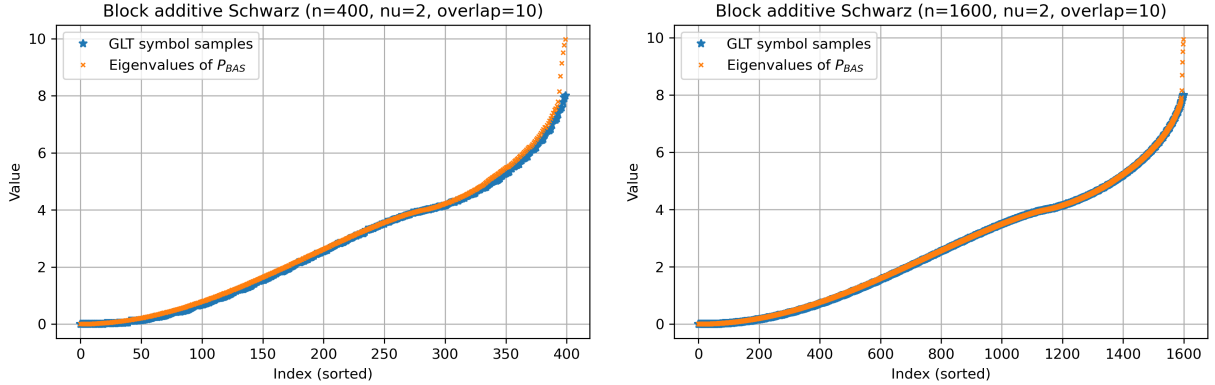


Figure 18: Comparison between the GLT symbol  $(1 + x^2)(2 - 2 \cos \theta)$  and the eigenvalues of the block additive Schwarz preconditioner  $P_{\text{BAS},n}^{(\nu)}$  with overlap  $o = 10$ . Left:  $n = 400$ ,  $\nu = 2$ . Right:  $n = 1600$ ,  $\nu = 2$ .

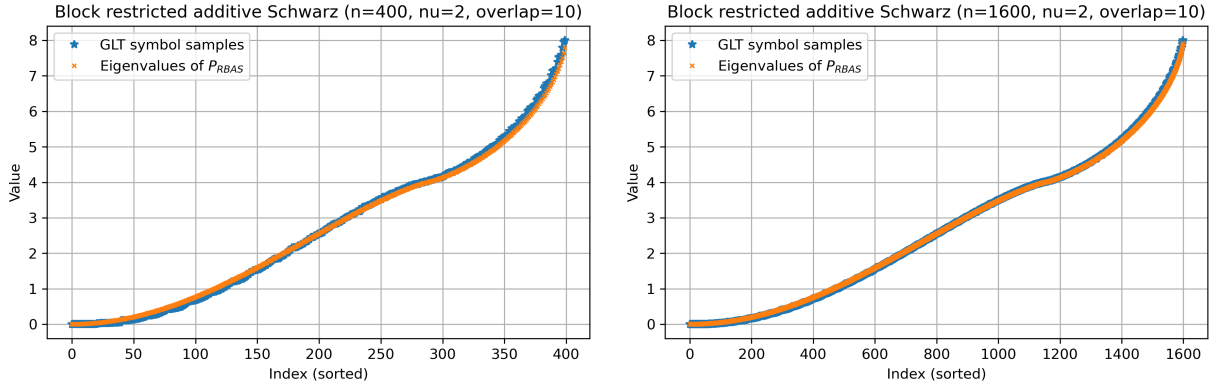


Figure 19: Comparison between the GLT symbol  $(1 + x^2)(2 - 2 \cos \theta)$  and the eigenvalues of the block restricted additive Schwarz preconditioner  $P_{\text{RBAS},n}^{(\nu)}$  with overlap  $o = 10$ . Left:  $n = 400$ ,  $\nu = 2$ . Right:  $n = 1600$ ,  $\nu = 2$ .

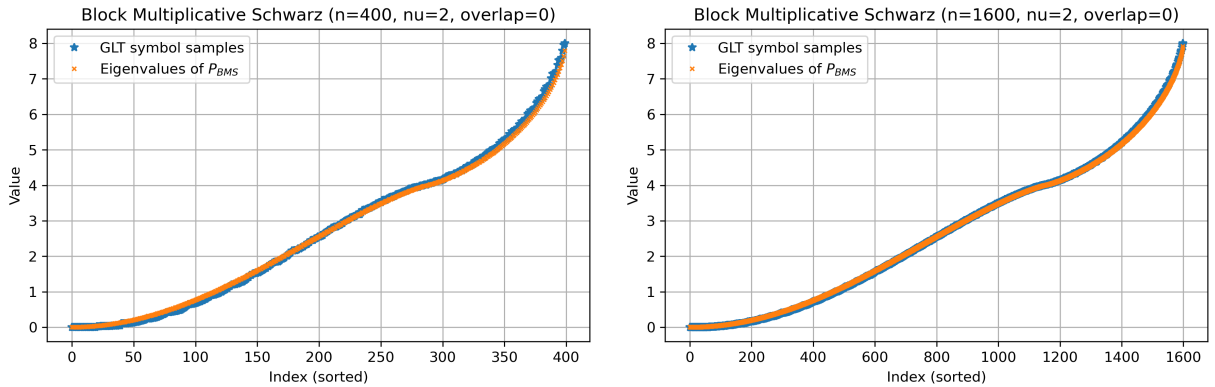


Figure 20: Comparison between the GLT symbol  $(1 + x^2)(2 - 2 \cos \theta)$  and the eigenvalues of the block multiplicative Schwarz preconditioner  $P_{\text{BMS},n}^{(\nu)}$  without overlap. Left:  $n = 400$ ,  $\nu = 2$ . Right:  $n = 1600$ ,  $\nu = 2$ .

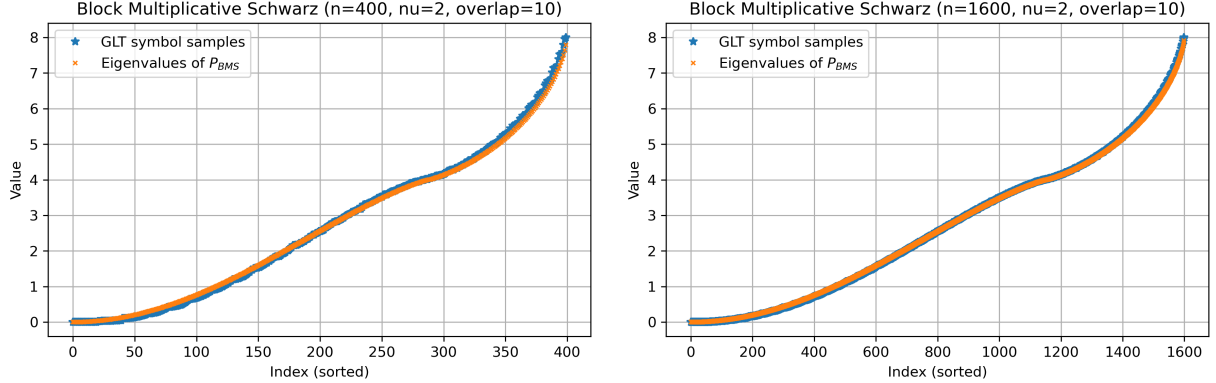


Figure 21: Comparison between the GLT symbol  $(1 + x^2)(2 - 2 \cos \theta)$  and the eigenvalues of the block multiplicative Schwarz preconditioner  $P_{BMS,n}^{(\nu)}$  with overlap  $o = 10$ . Left:  $n = 400, \nu = 2$ . Right:  $n = 1600, \nu = 2$ .

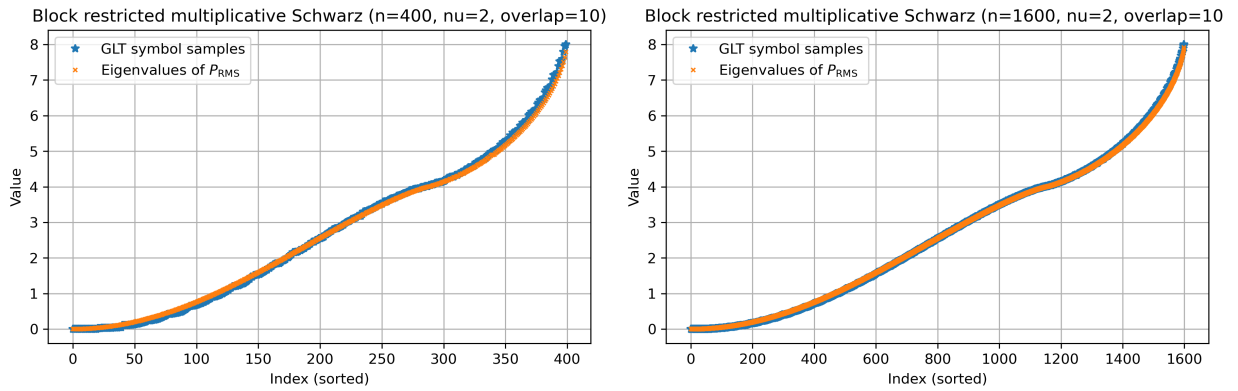


Figure 22: Comparison between the GLT symbol  $(1 + x^2)(2 - 2 \cos \theta)$  and the eigenvalues of the block restricted multiplicative Schwarz preconditioner  $P_{RMS,n}^{(\nu)}$  with overlap  $o = 10$ . Left:  $n = 400, \nu = 2$ . Right:  $n = 1600, \nu = 2$ .

In this case also the number  $s$  in item (A) is given by  $s = 1$ , we follow the program in item (B). The results are collected in Tables (23)–(26).

Method	$\nu$	$n = 40$	$n = 80$	$n = 160$	$n = 320$	$n = 640$	$n = 1280$	$n = 2560$
CG	1	40	80	160	320	640	1280	2560
	1	40	80	160	320	640	1280	2560
	1	40	80	160	320	640	1280	2560
	1	nac	80	160	320	640	1280	2560
PCG	2	4	4	4	4	4	4	4
	4	8	8	8	8	8	8	8
	8	10	14	16	16	16	17	17
	16	nac	15	22	28	32	33	33
GMRES	1	40	80	160	320	640	1280	2560
	1	40	80	160	320	640	1280	2560
	1	40	80	160	320	640	1280	2560
	1	nac	80	160	320	640	1280	2560
PGMRES	2	4	4	4	4	4	4	4
	4	8	8	8	8	8	8	13
	8	15	14	16	23	16	28	17
	16	nac	17	34	60	120	140	143

Table 23: Number of iterations for CG and GMRES with  $P_{BAS,n}^{(\nu)}(K_n)$ , with overlap  $o = 5$ .

<b>Method</b>	$\nu$	$n = 40$	$n = 80$	$n = 160$	$n = 320$	$n = 640$	$n = 1280$	$n = 2560$
CG	1	40	80	160	320	640	1280	2560
	1	40	80	160	320	640	1280	2560
	1	40	80	160	320	640	1280	2560
	1	40	80	160	320	640	1280	2560
PCG	2	40	80	160	320	640	1280	91
	4	40	80	160	320	640	105	39
	8	40	80	160	320	640	1280	152
	16	nac	80	160	320	640	1280	2560
GMRES	1	40	80	160	320	640	1280	2560
	1	40	80	160	320	640	1280	2560
	1	40	80	160	320	640	1280	2560
	1	40	80	160	320	640	1280	2560
PGMRES	2	2	2	2	2	2	2	3
	4	4	4	4	4	4	7	8
	8	5	8	8	8	8	16	9
	16	nac	12	16	16	16	17	21

Table 24: Number of iterations for CG and GMRES with  $P_{BMS,n}^{(\nu)}(K_n)$ , with overlap  $o = 5$ .

<b>Method</b>	<b>Metric</b>	$n = 40$	$n = 80$	$n = 160$	$n = 320$	$n = 640$	$n = 1280$	$n = 2560$
CG	1	40	80	160	320	640	1280	2560
	1	40	80	160	320	640	1280	2560
	1	40	80	160	320	640	1280	2560
	1	40	80	160	320	640	1280	2560
PCG	2	40	80	160	320	640	145	47
	4	40	80	160	124	79	60	56
	8	40	80	154	320	239	175	124
	16	nac	80	160	291	239	341	313
GMRES	1	40	80	160	320	640	1280	2560
	1	40	80	160	320	640	1280	2560
	1	40	80	160	320	640	1280	2560
	1	40	80	160	320	640	1280	2560
PGMRES	2	3	3	3	3	3	3	3
	4	7	7	7	7	7	7	14
	8	16	13	15	15	15	30	16
	16	nac	29	23	63	104	146	146

Table 25: Number of iterations for CG and GMRES with  $P_{BRAS,n}^{(\nu)}(K_n)$ , with overlap  $o = 5$ .

<b>Method</b>	<b>Metric</b>	$n = 40$	$n = 80$	$n = 160$	$n = 320$	$n = 640$	$n = 1280$	$n = 2560$
CG	1	40	80	160	320	640	1280	2560
	1	40	80	160	320	640	1280	2560
	1	40	80	160	320	640	1280	2560
	1	40	80	160	320	640	1280	2560
PCG	2	40	80	160	320	640	1280	2560
	4	40	80	160	320	640	1280	2560
	8	40	80	160	320	640	1280	2560
	16	nac	80	160	320	640	1280	2560
GMRES	1	40	80	160	320	640	1280	2560
	1	40	80	160	320	640	1280	2560
	1	40	80	160	320	640	1280	2560
	1	40	80	160	320	640	1280	2560
PGMRES	2	2	2	2	2	2	2	4
	4	4	4	4	4	4	7	8
	8	10	8	8	8	11	16	9
	16	nac	17	16	16	18	17	31

Table 26: Number of iterations for CG and GMRES with  $P_{BRMS,n}^{(\nu)}(K_n)$ , with overlap  $o = 5$ .

**Example 6.4** (High-order B-spline finite element discretization with  $s \geq 2$ ). We consider again the same model problem as in Example (6.3) with  $a(x) = 1$ . Here, however, instead of the standard hat functions, the basis functions  $\{\varphi_i\}_{i=1}^n$  are chosen as piecewise polynomials of degree  $p \geq 1$ . More precisely, we employ B-spline basis functions associated with a prescribed knot vector, which is defined as follows.  $\Xi = \{\xi_1, \xi_2, \dots, \xi_{n+p+1}\}$ , where repeated knots are allowed. Without loss of generality, we assume in the following that  $\xi_1 = 0$  and  $\xi_{n+p+1} = 1$ . We say that the knot vector  $\Xi$  is a  $p$ -open knot vector if the first and last knots are repeated  $p+1$  times, that is,  $\xi_1 = \dots = \xi_{p+1}$  and  $\xi_{n+1} = \dots = \xi_{n+p+1}$ . From the knot vector  $\Xi$ , B-spline basis functions of degree  $p$  (see, Figure (23)) are defined following the well-known Cox–de Boor recursive formula. We start with piecewise constants ( $p = 0$ ):

$$B_{i,0}(\xi) = \begin{cases} 1, & \text{if } \xi_i \leq \xi < \xi_{i+1}, \\ 0, & \text{otherwise,} \end{cases} \quad (34)$$

and for  $p \geq 1$  the B-spline basis functions are defined by the recursion

$$B_{i,p}(\xi) = \frac{\xi - \xi_i}{\xi_{i+p} - \xi_i} B_{i,p-1}(\xi) + \frac{\xi_{i+p+1} - \xi}{\xi_{i+p+1} - \xi_{i+1}} B_{i+1,p-1}(\xi), \quad (35)$$

This construction gives a set of  $n$  B-spline basis functions  $\{B_{i,p}\}_{i=1}^n$  satisfying the following properties: (i) **Non-negativity**:  $B_{i,p}(\xi) \geq 0$  for all  $\xi \in [0, 1]$ ; (ii) **Partition of unity**:  $\sum_{i=1}^n B_{i,p}(\xi) = 1$  for all  $\xi \in [0, 1]$ ; (iii) **Local support**:  $B_{i,p}(\xi) = 0$  for all  $\xi \notin [\xi_i, \xi_{i+p+1}]$ , and  $B_{i,p}(\xi) = 0$  for all  $\xi \in (\xi_r, \xi_{r+1})$  whenever  $i \notin \{r-p, r-p+1, \dots, r\}$ ; (iv) **Translation and scaling invariance**: if  $\Xi = \{\xi_i\}_i$  is a knot vector and  $\alpha, \beta \in \mathbb{R}$  with  $\alpha \neq 0$ , then for the transformed knot vector  $\alpha\Xi + \beta := \{\alpha\xi_i + \beta\}_i$ , the associated B-spline basis functions satisfy  $B_{i,p}(\alpha\Xi + \beta) = B_{i,p}(\Xi)$ .

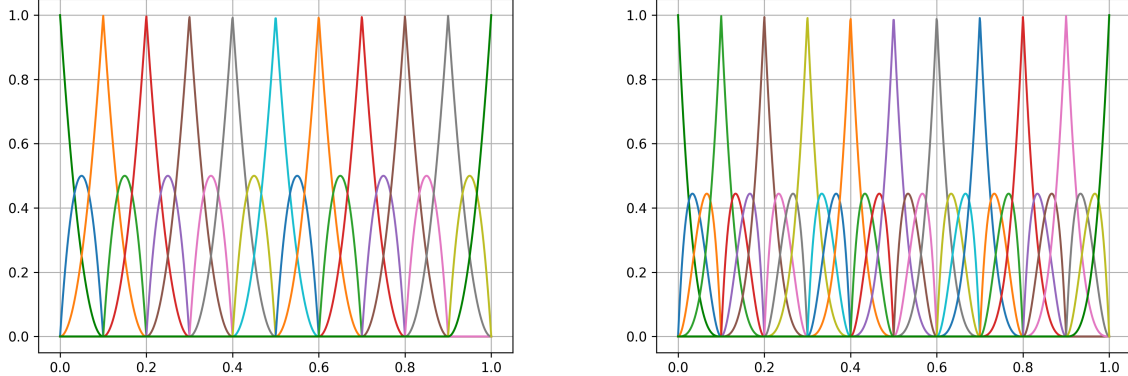


Figure 23:  $C^0$  B-splines constructed using the open knot vector  $\Xi := \left\{ \underbrace{0, \dots, 0}_{p+1}, \underbrace{\frac{1}{n}, \dots, \frac{1}{n}}_p, \dots, \underbrace{\frac{n-1}{n}, \dots, \frac{n-1}{n}}_p, \underbrace{1, \dots, 1}_{p+1} \right\}$ , with  $n = 10$ . Left:  $p = 2$ ; right:  $p = 3$ .

Here, we consider only quadratic and cubic  $C^0$ -continuous B-spline bases, see Figure (23). These bases are constructed from open, uniform knot vectors with repeated interior knots ( $p$  times). For the quadratic case ( $p = 2$ ), the open knot vector is defined as  $\Xi := \{0, 0, 0, \frac{1}{n}, \frac{1}{n}, \frac{2}{n}, \frac{2}{n}, \dots, \frac{n-1}{n}, \frac{n-1}{n}, 1, 1, 1\}$ , which yields a quadratic  $C^0$ -continuous B-spline basis. For the cubic case ( $p = 3$ ), the corresponding knot vector reads  $\Xi := \{0, 0, 0, 0, \frac{1}{n}, \frac{1}{n}, \frac{1}{n}, \frac{2}{n}, \frac{2}{n}, \frac{2}{n}, \dots, \frac{n-1}{n}, \frac{n-1}{n}, \frac{n-1}{n}, 1, 1, 1, 1\}$ , leading to a cubic  $C^0$ -continuous B-spline basis. The corresponding basis functions are illustrated in Figures (23). We begin with the case  $p = 2$ . According to the notation introduced above, the entries of the stiffness matrix  $K_n$  are defined by

$$(K_n)_{ij} := \int_0^1 B'_{i,2}(\xi) B'_{j,2}(\xi) d\xi, \quad i, j = 2, \dots, 2n.$$

In this setting, the theory of GLT sequences yields the following result:

$$\left\{ \frac{1}{n} K_n \right\}_n \sim_{\text{GLT}} f(\theta) := \frac{1}{3} \begin{bmatrix} 4 & -2 - 2e^{i\theta} \\ -2 - 2e^{-i\theta} & 8 - 4 \cos \theta \end{bmatrix}. \quad (36)$$

The theoretical analysis developed in this paper also confirms that all classical block preconditioners under consideration exhibit the predicted asymptotic behavior. More precisely, for each preconditioner  $P_{\star,n}^{(\nu)}$ , the associated matrix sequence satisfies

$$\{P_{\star,n}^{(\nu)}\}_n \sim_{\text{GLT}} f(\theta) := \frac{1}{3} \begin{bmatrix} 4 & -2 - 2e^{i\theta} \\ -2 - 2e^{-i\theta} & 8 - 4 \cos \theta \end{bmatrix}, \quad \star \in \{\text{BJ, BAS, BRAS, BGS, BMS, BRMS}\}.$$

Numerical experiments supporting this theoretical prediction are performed following the procedure described in item (C). The corresponding results are reported in Figures (24)–(26).

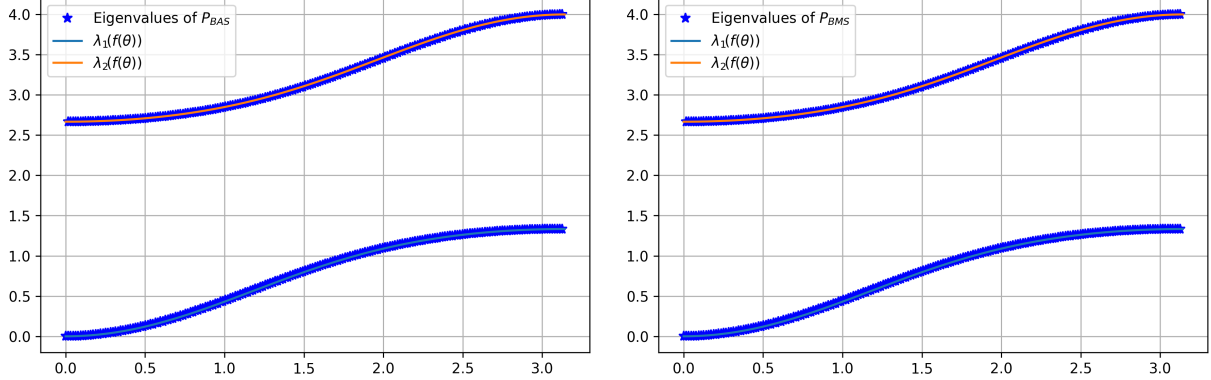


Figure 24: Quadratic  $C^0$  B-spline discretization: Comparison between the GLT symbol  $f(\theta)$  and the eigenvalues of the block Schwarz preconditioners without overlap,  $\nu = 2$ , and  $n = 200$ . Left: additive  $P_{\text{BAS},n}^{(\nu)}$ ; Right: multiplicative  $P_{\text{BMS},n}^{(\nu)}$ .

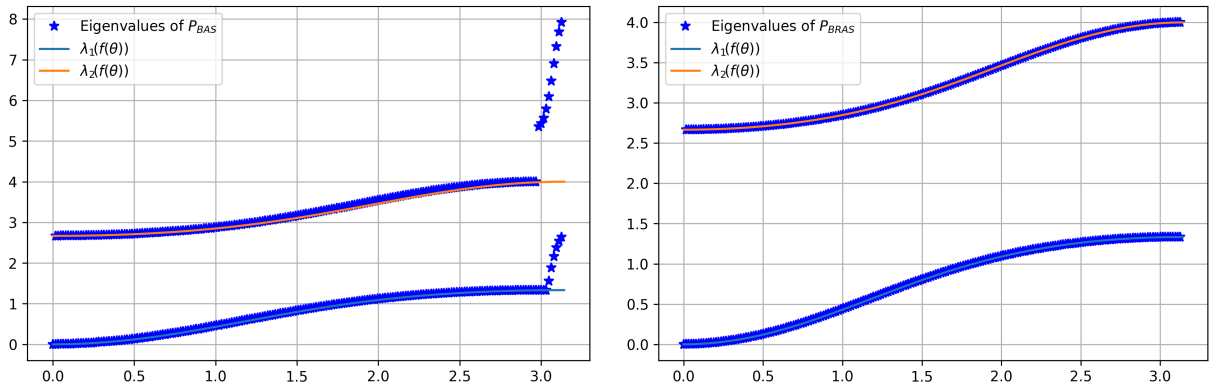


Figure 25: Quadratic  $C^0$  B-spline discretization: Comparison between the GLT symbol  $f(\theta)$  and the eigenvalues of the block Schwarz preconditioners with overlap  $o = 10$ ,  $\nu = 2$ , and  $n = 200$ . Left: additive  $P_{\text{BAS},n}^{(\nu)}$ ; Right: restricted additive  $P_{\text{BRAS},n}^{(\nu)}$ .

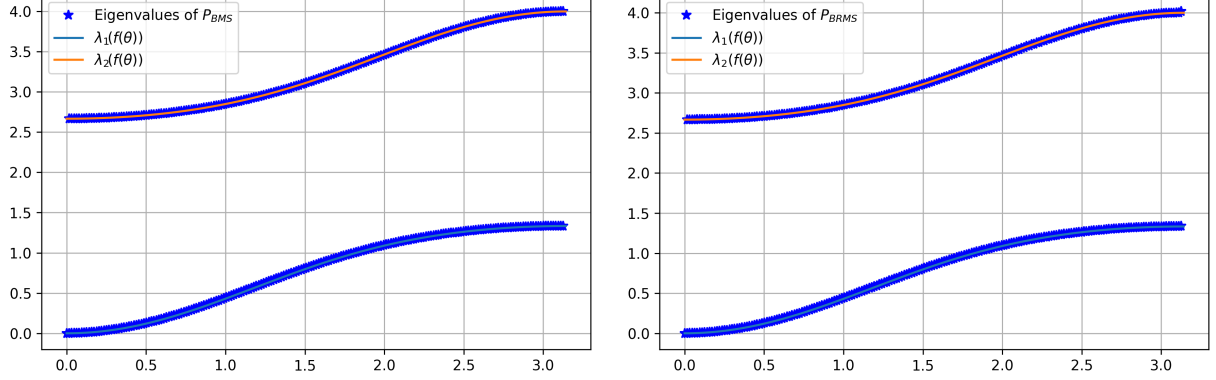


Figure 26: Quadratic  $C^0$  B-spline discretization: Comparison between the GLT symbol  $\mathbf{f}(\theta)$  and the eigenvalues of the block Schwarz preconditioners with overlap  $o = 10$ ,  $\nu = 2$ , and  $n = 200$ . Left: multiplicative  $P_{BMS,n}^{(\nu)}$ ; Right: restricted multiplicative  $P_{BRMS,n}^{(\nu)}$ .

In the case  $p = 2$ , the parameter  $s$  introduced in item (A) equals 2. Accordingly, we perform the numerical procedure described in item (B). The resulting data are reported in Tables (27)–(30).

Method	$\nu$	$n = 40$	$n = 80$	$n = 160$	$n = 320$	$n = 640$	$n = 1280$	$n = 2560$
CG	1	35	63	119	229	446	877	1737
	1	35	63	119	229	446	877	1737
	1	35	63	119	229	446	877	1737
	1	35	63	119	229	446	877	1737
PCG	2	4	4	4	4	4	4	4
	4	8	8	8	8	8	8	8
	8	14	16	16	16	16	17	17
	16	nac	22	27	32	33	33	34
GMRES	1	79	159	319	639	1279	2559	5119
	1	79	159	319	639	1279	2559	5119
	1	79	159	319	639	1279	2559	5119
	1	79	159	319	639	1279	2559	5119
PGMRES	2	4	4	4	4	4	7	7
	4	8	8	8	8	8	18	15
	8	15	17	16	16	20	38	39
	16	nac	28	35	51	53	55	67

Table 27: Number of iterations for CG and GMRES with  $P_{BAS,n}^{(\nu)}(K_n)$ , with overlap  $o = 5$

Method	Metric	$n = 40$	$n = 80$	$n = 160$	$n = 320$	$n = 640$	$n = 1280$	$n = 2560$
CG	1	35	63	119	229	446	877	1737
	1	35	63	119	229	446	877	1737
	1	35	63	119	229	446	877	1737
	1	nac	63	119	229	446	877	1737
PCG	2	79	159	319	639	1279	47	20
	4	79	159	319	225	72	49	34
	8	79	159	319	639	1279	106	62
	16	nac	159	319	639	1279	2559	455
GMRES	1	79	159	319	639	1279	2559	5119
	1	79	159	319	639	1279	2559	5119
	1	79	159	319	639	1279	2559	5119
	1	nac	159	319	639	1279	2559	5119
PGMRES	2	2	2	2	2	2	2	3
	4	4	4	4	4	4	8	8
	8	8	8	8	8	13	9	9
	16	nac	15	16	16	17	17	18

Table 28: Number of iterations for CG and GMRES with  $P_{BMS,n}^{(\nu)}(K_n)$ , with overlap  $o = 5$ .

Method	Metric	$n = 40$	$n = 80$	$n = 160$	$n = 320$	$n = 640$	$n = 1280$	$n = 2560$
CG	1	35	63	119	229	446	877	1737
	1	35	63	119	229	446	877	1737
	1	35	63	119	229	446	877	1737
	1	35	63	119	229	446	877	1737
PCG	2	79	159	319	639	92	82	32
	4	79	48	146	45	43	42	37
	8	79	159	319	169	138	74	114
	16	nac	159	319	170	311	265	183
GMRES	1	79	159	319	639	1279	2559	5119
	1	79	159	319	639	1279	2559	5119
	1	79	159	319	639	1279	2559	5119
	1	79	159	319	639	1279	2559	5119
PGMRES	2	3	3	3	3	3	3	3
	4	7	7	7	7	7	7	11
	8	15	16	15	15	21	27	28
	16	nac	36	49	38	44	72	68

Table 29: Number of iterations for CG and GMRES with  $P_{BRAS,n}^{(\nu)}(K_n)$ , with overlap  $o = 5$ .

Method	$\nu$	$n = 40$	$n = 80$	$n = 160$	$n = 320$	$n = 640$	$n = 1280$	$n = 2560$
CG	1	35	63	119	229	446	877	1737
	1	35	63	119	229	446	877	1737
	1	35	63	119	229	446	877	1737
	1	35	63	119	229	446	877	1737
PCG	2	79	159	319	639	1279	2559	5119
	4	79	159	319	639	1279	2559	5119
	8	79	159	319	639	1279	2559	5119
	16	nac	159	319	639	1279	2559	5119
GMRES	1	79	159	319	639	1279	2559	5119
	1	79	159	319	639	1279	2559	5119
	1	79	159	319	639	1279	2559	5119
	1	79	159	319	639	1279	2559	5119
PGMRES	2	2	2	2	2	2	2	4
	4	4	4	4	4	4	8	8
	8	8	8	8	8	16	9	9
	16	nac	16	16	16	17	17	18

Table 30: Number of iterations for CG and GMRES with  $P_{BRMS,n}^{(\nu)}(K_n)$ , with overlap  $o = 5$ .

We now turn to the cubic case. According to the notation introduced above, the entries of the stiffness matrix  $K_n$  are given by

$$(K_n)_{ij} := \int_0^1 B'_{i,3}(\xi) B'_{j,3}(\xi) d\xi, \quad i, j = 2, \dots, 3n.$$

In this case, the corresponding matrix sequence again falls within the Generalized Locally Toeplitz (GLT) class. More precisely, one has

$$\left\{ \frac{1}{n} K_n \right\}_n \sim_{\text{GLT}} f(\theta) := \frac{1}{10} \begin{bmatrix} 12 & 3 & -6 - 9e^{i\theta} \\ 3 & 12 & -9 - 6e^{i\theta} \\ -6 - 9e^{-i\theta} & -9 - 6e^{-i\theta} & 36 - 6 \cos \theta \end{bmatrix}. \quad (37)$$

Moreover, the theoretical framework developed in this work applies directly to this setting, implying that all classical block preconditioners considered herein share the same asymptotic spectral behavior. That is,

$$\{P_{\star,n}^{(\nu)}\}_n \sim_{\text{GLT}} f(\theta) = \frac{1}{10} \begin{bmatrix} 12 & 3 & -6 - 9e^{i\theta} \\ 3 & 12 & -9 - 6e^{i\theta} \\ -6 - 9e^{-i\theta} & -9 - 6e^{-i\theta} & 36 - 6 \cos \theta \end{bmatrix}, \quad \star \in \{\text{BJ, BAS, BRAS, BGS, BMS, BRMS}\}.$$

Numerical experiments validating these theoretical findings are carried out according to the procedure described in item (C). The corresponding results are reported in Figures (27)–(29).

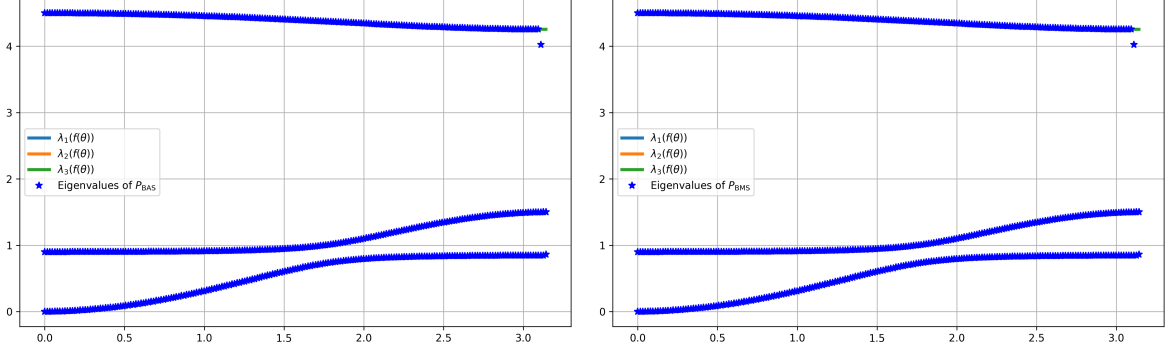


Figure 27: Cubic  $C^0$  B-spline discretization: Comparison between the GLT symbol  $f(\theta)$  and the eigenvalues of the block Schwarz preconditioners without overlap,  $\nu = 2$ , and  $n = 200$ . Left: additive  $P_{\text{BAS},n}^{(\nu)}$ ; Right: multiplicative  $P_{\text{BMS},n}^{(\nu)}$ .

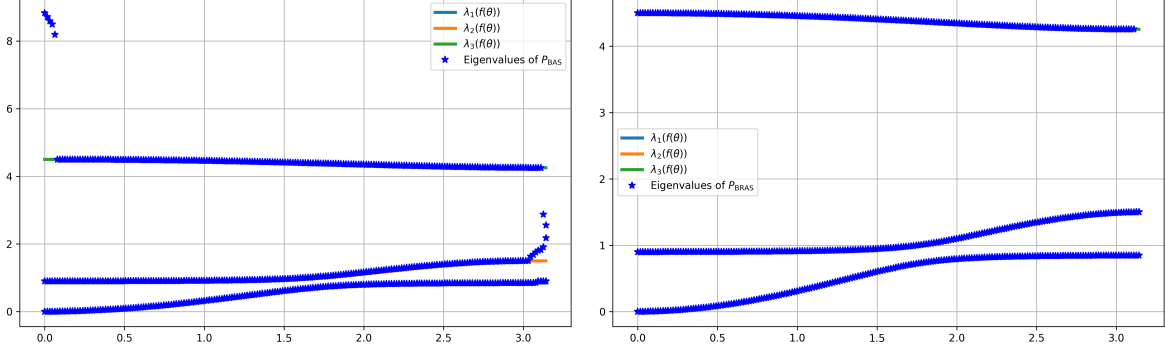


Figure 28: Cubic  $C^0$  B-spline discretization: Comparison between the GLT symbol  $f(\theta)$  and the eigenvalues of the block Schwarz preconditioners with overlap  $o = 10$ ,  $\nu = 2$ , and  $n = 200$ . Left: additive  $P_{\text{BAS},n}^{(\nu)}$ ; Right: restricted additive  $P_{\text{BRAS},n}^{(\nu)}$ .

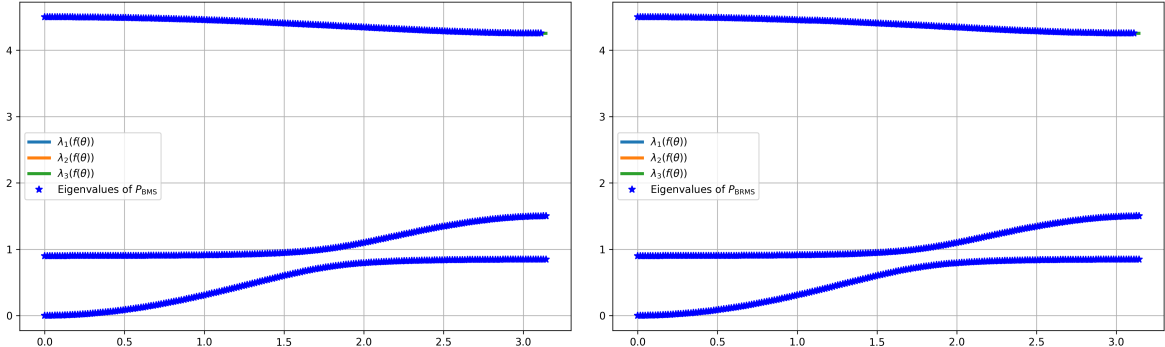


Figure 29: Cubic  $C^0$  B-spline discretization: Comparison between the GLT symbol  $f(\theta)$  and the eigenvalues of the block Schwarz preconditioners with overlap  $o = 10$ ,  $\nu = 2$ , and  $n = 200$ . Left: multiplicative  $P_{\text{BMS},n}^{(\nu)}$ ; Right: restricted multiplicative  $P_{\text{BRMS},n}^{(\nu)}$ .

In the case  $p = 3$ , the parameter  $s$  introduced in item (A) equals 3. Accordingly, we perform the numerical procedure described in item (B). The resulting data are reported in Tables (31)–(34).

Method	$\nu$	$n = 40$	$n = 80$	$n = 160$	$n = 320$	$n = 640$	$n = 1280$	$n = 2560$
CG	1	38	70	131	252	494	975	1937
	1	38	70	131	252	494	975	1937
	1	38	70	131	252	494	975	1937
	1	38	70	131	252	494	975	1937
PCG	2	4	4	4	4	4	4	4
	4	8	8	8	8	8	8	9
	8	14	16	16	16	17	17	17
	16	19	23	30	32	33	33	34
GMRES	1	119	239	479	959	1919	3839	7679
	1	119	239	479	959	1919	3839	7679
	1	119	239	479	959	1919	3839	7679
	1	119	239	479	959	1919	3839	7679
PGMRES	2	4	4	4	4	7	7	7
	4	8	8	8	8	13	12	13
	8	19	16	16	16	39	17	33
	16	20	39	52	53	56	67	65

Table 31: Number of iterations for CG and GMRES with  $P_{BAS,n}^{(\nu)}(K_n)$ , with overlap  $o = 5$ .

Method	$\nu$	$n = 40$	$n = 80$	$n = 160$	$n = 320$	$n = 640$	$n = 1280$	$n = 2560$
CG	2	38	70	131	252	494	975	1937
	4	38	70	131	252	494	975	1937
	8	38	70	131	252	494	975	1937
	16	38	70	131	252	494	975	1937
PCG	2	119	239	479	959	108	34	20
	4	119	239	332	69	46	36	26
	8	119	239	479	959	398	120	59
	16	119	239	479	959	1919	3839	264
GMRES	1	119	239	479	959	1919	3839	7679
	1	119	239	479	959	1919	3839	7679
	1	119	239	479	959	1919	3839	7679
	1	119	239	479	959	1919	3839	7679
PGMRES	2	2	2	2	2	2	2	3
	4	4	4	4	4	7	8	8
	8	8	8	8	8	16	9	9
	16	12	16	16	26	17	30	18

Table 32: Number of iterations for CG and GMRES with  $P_{BMS,n}^{(\nu)}(K_n)$ , with overlap  $o = 5$ .

Method	$\nu$	$n = 40$	$n = 80$	$n = 160$	$n = 320$	$n = 640$	$n = 1280$	$n = 2560$
CG	1	38	70	131	252	494	975	1937
	1	38	70	131	252	494	975	1937
	1	38	70	131	252	494	975	1937
	11	38	70	131	252	494	975	1937
PCG	2	119	239	479	710	37	104	241
	4	75	239	87	41	41	78	46
	8	119	239	352	108	91	86	100
	16	119	239	270	189	392	178	146
GMRES	1	119	239	479	959	1919	3839	7679
	1	119	239	479	959	1919	3839	7679
	1	119	239	479	959	1919	3839	7679
	1	119	239	479	959	1919	3839	7679
PGMRES	2	3	3	3	3	3	3	5
	4	7	7	7	7	10	10	12
	8	14	15	15	15	30	16	16
	16	32	38	40	47	71	93	66

Table 33: Number of iterations for CG and GMRES with  $P_{BRAS,n}^{(\nu)}(K_n)$ , with overlap  $o = 5$ .

Method	$\nu$	$n = 40$	$n = 80$	$n = 160$	$n = 320$	$n = 640$	$n = 1280$	$n = 2560$
CG	1	38	70	131	252	494	975	1937
	1	38	70	131	252	494	975	1937
	1	38	70	131	252	494	975	1937
	1	38	70	131	252	494	975	1937
PCG	2	119	239	479	959	1919	3839	7679
	4	119	239	479	959	1919	3839	7679
	8	119	239	479	959	1919	3839	7679
	16	119	239	479	959	1919	3839	7679
GMRES	1	119	239	479	959	1919	3839	7679
	1	119	239	479	959	1919	3839	7679
	1	119	239	479	959	1919	3839	7679
	1	119	239	479	959	1919	3839	7679
PGMRES	2	2	2	2	2	2	2	3
	4	4	4	4	4	7	8	8
	8	8	8	8	11	16	9	9
	16	15	16	16	29	17	33	18

Table 34: Number of iterations for CG and GMRES with  $P_{BRAS,n}^{(\nu)}(K_n)$ , with overlap  $o = 5$ .

**Remark 6.2.** Regarding the numerical findings, it is important to note that the block additive Schwarz preconditioner exhibits some outliers in the spectrum. In contrast, the block restricted additive Schwarz preconditioner effectively removes these outliers by using the restricted prolongation operator. This observation provides further evidence, in agreement with GLT theory, that the block additive Schwarz preconditioner is not intended to be used as a stand-alone iterative solver, but rather is designed to act effectively as a preconditioning tool.

## 6.2 The 2D Setting

Regarding item (A), we consider  $d = 2$  i.e

- Let  $\{A_n\}_n \sim_{GLT} \kappa$  be a fixed GLT sequence, where each  $A_n$  is an invertible square matrix of size  $n^2 s \times n^2 s$ , for some fixed positive integer  $s$ , and  $\kappa : [0, 1]^2 \times [-\pi, \pi]^2 \rightarrow \mathbb{C}^{s \times s}$  is a measurable matrix-valued function.

In what follows, we restrict our attention to the two-dimensional model problem with high-order finite elements:

$$\begin{cases} -\nabla \cdot (a(x) \nabla u(x)) = f(x), & x \in \Omega := (0, 1)^2, \\ u(x) = 0, & x \in \partial\Omega, \end{cases} \quad (38)$$

where  $a(x)$  is a diffusion coefficient and  $f(x)$  is a source term. We assume  $a(x) \in L^\infty(\Omega)$ ,  $a(x) \geq a_{\min} > 0$ , and  $f \in L^2(\Omega)$ . The weak formulation reads:

$$\text{Find } u \in H_0^1(\Omega) \text{ such that } \int_{\Omega} a(x) \nabla u(x) \cdot \nabla v(x) dx = \int_{\Omega} f(x) v(x) dx \quad \forall v \in H_0^1(\Omega).$$

A multivariate B-spline basis is constructed as the tensor product of univariate B-splines:

$$B_{\mathbf{j}, \mathbf{p}}(\mathbf{x}) := \bigotimes_{i=1}^2 B_{j_i, p_i}(x_i),$$

where  $B_{j_i, p_i}$  is the univariate B-spline of degree  $p_i$  in the  $i$ -th direction, and  $\mathbf{j} = (j_1, j_2)$ ,  $\mathbf{p} = (p_1, p_2)$ . The corresponding discrete subspace of  $H_0^1(\Omega)$  is defined by

$$V_h := \text{span} \left\{ B_{\mathbf{j}, \mathbf{p}} := \bigotimes_{i=1}^2 B_{j_i, p_i} \mid j_i = 1, \dots, n_i, j = 1, 2 \right\}.$$

Finally, the entries of the (weighted) stiffness matrix are given by

$$(K_n^a)_{\mathbf{i}, \mathbf{j}} = \int_0^1 \int_0^1 a(x_1, x_2) \left( \partial_{x_1} B_{i_1, p_1} \partial_{x_1} B_{j_1, p_1} B_{i_2, p_2} B_{j_2, p_2} + B_{i_1, p_1} B_{j_1, p_1} \partial_{x_2} B_{i_2, p_2} \partial_{x_2} B_{j_2, p_2} \right) dx_1 dx_2. \quad (39)$$

Here, we consider  $C^{p-1}$  B-spline bases, corresponding to open knot vectors without interior repetition. The parameter  $s$  introduced in item (A) is set to  $s = 1$ , we follow the numerical procedure described in item (B). The results are

summarized in Tables (35)–(38) for  $a(x_1, x_2) = 1$  with  $p_1 = p_2 = 2$ , and in Tables (39)–(42) for  $a(x_1, x_2) = 1 + x_1 + x_2$  with  $p_1 = p_2 = 3$ .

Method	$\nu$	$n^2 = 8 \times 8$	$n^2 = 16 \times 16$	$n^2 = 32 \times 32$	$n^2 = 64 \times 64$
CG	1	14	18	23	41
	1	14	18	23	41
	1	14	18	23	41
	1	14	18	23	41
PCG	2	4	7	11	16
	4	8	9	14	21
	8	nac	11	18	26
	16	nac	nac	26	36
GMRES	1	14	18	23	97
	1	14	18	23	97
	1	14	18	23	97
	1	14	18	23	97
PGMRES	2	4	7	11	18
	4	8	9	14	23
	8	nac	12	19	31
	16	nac	nac	27	45

Table 35: Number of iterations for CG and GMRES with  $P_{BAS,n}^{(\nu)}(K_n^1)$ , with overlap  $o = 20$ .

Method	$\nu$	$n^2 = 8 \times 8$	$n^2 = 16 \times 16$	$n^2 = 32 \times 32$	$n^2 = 64 \times 64$
CG	1	14	18	23	41
	1	14	18	23	41
	1	14	18	23	41
	1	14	18	23	41
PCG	2	4	289	78	82
	4	4	289	1089	143
	8	nac	289	1089	4225
	16	nac	nac	1089	4225
GMRES	1	14	18	23	97
	1	14	18	23	97
	1	14	18	23	97
	1	14	18	23	97
PGMRES	2	2	4	6	10
	4	2	5	8	13
	8	nac	6	13	17
	16	nac	nac	19	26

Table 36: Number of iterations for CG and GMRES with  $P_{BMS,n}^{(\nu)}(K_n^1)$ , with overlap  $o = 20$ .

Method	$\nu$	$n^2 = 8 \times 8$	$n^2 = 16 \times 16$	$n^2 = 32 \times 32$	$n^2 = 64 \times 64$
CG	1	14	18	23	41
	1	14	18	23	41
	1	14	18	23	41
	1	14	18	23	41
PCG	2	6	289	23	27
	4	5	109	48	40
	8	nac	289	149	4225
	16	nac	nac	1089	4225
GMRES	1	14	18	23	97
	1	14	18	23	97
	1	14	18	23	97
	1	14	18	23	97
PGMRES	2	4	7	11	18
	4	5	8	14	23
	8	nac	10	19	31
	16	nac	nac	25	45

Table 37: Number of iterations for CG and GMRES with  $P_{BRAS,n}^{(\nu)}(K_n^1)$ , with overlap  $o = 20$ .

Method	$\nu$	$n^2 = 8 \times 8$	$n^2 = 16 \times 16$	$n^2 = 32 \times 32$	$n^2 = 64 \times 64$
CG	1	14	18	23	41
	1	14	18	23	41
	1	14	18	23	41
	1	14	18	23	41
PCG	2	6	289	378	124
	4	8	289	1089	747
	8	nac	289	1089	4225
	16	nac	nac	1089	4225
GMRES	1	14	18	23	97
	1	14	18	23	97
	1	14	18	23	97
	1	14	18	23	97
PGMRES	2	3	4	7	10
	4	3	6	9	13
	8	nac	9	12	17
	16	nac	nac	22	25

Table 38: Number of iterations for CG and GMRES with  $P_{BRMS,n}^{(\nu)}(K_n^1)$ , with overlap  $o = 20$ .

Method	$\nu$	$n^2 = 8 \times 8$	$n^2 = 16 \times 16$	$n^2 = 32 \times 32$	$n^2 = 64 \times 64$
CG	1	21	26	37	75
	1	21	26	37	75
	1	21	26	37	75
	1	21	26	37	75
PCG	2	4	7	11	17
	4	8	10	14	23
	8	nac	11	19	29
	16	nac	nac	28	40
GMRES	1	21	27	53	177
	1	21	27	53	177
	1	21	27	53	177
	1	21	2	53	177
PGMRES	2	4	7	12	19
	4	8	11	15	24
	8	nac	12	21	32
	16	nac	nac	30	49

Table 39: Number of iterations for CG and GMRES with  $P_{BAS,n}^{(\nu)}(K_n^{1+x_1+x_2})$ , with overlap  $o = 20$ 

Method	$\nu$	$n^2 = 8 \times 8$	$n^2 = 16 \times 16$	$n^2 = 32 \times 32$	$n^2 = 64 \times 64$
CG	1	21	26	37	75
	1	21	26	37	75
	1	21	26	37	75
	1	21	26	37	75
PCG	2	4	289	102	75
	4	4	289	1089	177
	8	nac	289	1089	4225
	16	nac	nac	1089	4225
GMRES	1	21	27	53	177
	1	21	27	53	177
	1	21	27	53	177
	1	21	27	53	177
PGMRES	2	2	4	6	10
	4	2	6	9	13
	8	nac	6	13	17
	16	nac	nac	19	29

Table 40: Number of iterations for CG and GMRES with  $P_{BMS,n}^{(\nu)}(K_n^{1+x_1+x_2})$ , with overlap  $o = 20$ .

Method	$\nu$	$n^2 = 8 \times 8$	$n^2 = 16 \times 16$	$n^2 = 32 \times 32$	$n^2 = 64 \times 64$
CG	1	21	26	37	75
	1	21	26	37	75
	1	21	26	37	75
	1	21	26	37	75
PCG	2	6	289	22	25
	4	5	109	43	40
	8	nac	289	149	4225
	16	nac	nac	1089	4045
GMRES	1	21	27	53	177
	1	21	27	53	177
	1	21	27	53	177
	1	21	27	53	177
PGMRES	2	4	7	11	18
	4	5	8	15	23
	8	nac	12	20	31
	16	nac	nac	26	50

Table 41: Number of iterations for CG and GMRES with  $P_{BRAS,n}^{(\nu)}(K_n^{1+x_1+x_2})$ , with overlap  $o = 20$ .

Method	$\nu$	$n^2 = 8 \times 8$	$n^2 = 16 \times 16$	$n^2 = 32 \times 32$	$n^2 = 64 \times 64$
CG	1	21	26	37	75
	1	21	26	37	75
	1	21	26	37	75
	1	21	26	37	75
PCG	2	6	289	1089	144
	4	9	289	1089	1084
	8	nac	289	1089	4225
	16	nac	nac	1089	4225
GMRES	1	21	27	53	177
	1	21	27	53	177
	1	21	27	53	177
	1	21	27	53	177
PGMRES	2	3	4	6	10
	4	3	6	9	13
	8	nac	9	12	17
	16	nac	nac	21	27

Table 42: Number of iterations for CG and GMRES with  $P_{BRAS,n}^{(\nu)}(K_n^{1+x_1+x_2})$ , with overlap  $o = 20$ .

## 7 Conclusions and perspectives

Our main results establish that for any GLT sequence  $\{A_n\}_n \sim_{GLT} \kappa$ , any block additive or multiplicative preconditioner, with or without overlap,  $\{P_n\}_n$  also forms a GLT sequence with the same symbol  $\kappa$ , provided that the number of blocks  $\nu$  remains fixed independently of  $n$ . This provides a unified theoretical justification for the effectiveness of Schwarz-type preconditioners in the GLT framework.

These results open several avenues for future research.

- First, it is important to extend these theorems to the multidimensional case for general domains and graded meshes, where the underlying GLT sequences correspond to higher-dimensional discretizations of partial differential operators.
- Second, the behavior of optimized Schwarz methods [28] in the GLT setting remains to be investigated, particularly regarding how the choice of optimized transmission conditions affects the spectral properties of the preconditioned matrix-sequences.
- Third, understanding the continuous-level counterpart of these results, i.e., the link between GLT symbols and the associated continuous operators, could provide deeper insights into the convergence and efficiency of domain decomposition methods.

- Fourth, the present work has a lot of relations with the open problems concerning the blocking idea as proposed and studied in [2, 3, 4, 5, 13]; for future steps see in particular the Research Project 8 in [52] and references therein.
- Finally, in the context of IgA, where parametrization introduces additional structure and coupling in the system matrices [43], it is crucial to examine how these preconditioners behave and whether GLT-based spectral predictions remain valid.

Addressing the questions listed above will broaden the applicability of GLT-based analysis to a wider class of preconditioning strategies and discretization methods.

## References

- [1] A. Adriani, A.J.A. Schiavoni-Piazza, S. Serra-Capizzano, C. Tablino-Possio. Revisiting the notion of approximating class of sequences for handling approximated PDEs on moving or unbounded domains. *Electronic Transactions on Numerical Analysis*, 63:424–451, 2025.
- [2] A. Adriani, I. Furci, C. Garoni, S. Serra-Capizzano. Spectral and singular value distribution of sequences of block matrices with rectangular Toeplitz blocks. Part I: Asymptotically rational block size ratios. *Journal of Numerical Mathematics*, in press.
- [3] A. Adriani, C. Garoni, S. Serra-Capizzano. Spectral and singular value distribution of sequences of block matrices with rectangular Toeplitz blocks. Part II: Asymptotically irrational block size ratios. *Journal of Numerical Mathematics*, in press.
- [4] N. Barakitis, P. Ferrari, I. Furci, S. Serra-Capizzano. An extradimensional approach for distributional results: the case of  $2 \times 2$  block Toeplitz structures. *Mathematical modeling with modern applications*, 61–78, Springer Proceedings in Mathematics & Statistics, 497, Springer, Cham, 2025.
- [5] N. Barakitis, M. Donatelli, S. Ferri, V. Loi, S. Serra-Capizzano, R. L. Sormani. Blocking structures, approximation, and preconditioning. *Numerical Algorithms*, 100(4):1893–1927, 2025.
- [6] G. Barbarino. A systematic approach to reduced GLT. *BIT Numerical Mathematics*, 62(3):681–743, 2022.
- [7] G. Barbarino, C. Garoni, M. Mazza, S. Serra-Capizzano. Rectangular GLT sequences. *Electronic Transactions on Numerical Analysis*, 55:585–617, 2022.
- [8] G. Barbarino, C. Garoni, S. Serra-Capizzano. Block generalized locally Toeplitz sequences: theory and applications in the unidimensional case. *Electronic Transactions on Numerical Analysis*, 53:28–112, 2020.
- [9] G. Barbarino, C. Garoni, S. Serra-Capizzano. Block generalized locally Toeplitz sequences: theory and applications in the multidimensional case. *Electronic Transactions on Numerical Analysis*, 53:113–226, 2020.
- [10] G. Barbarino, S. Serra-Capizzano. Non-Hermitian perturbations of Hermitian matrix-sequences and applications to the spectral analysis of the numerical approximation of partial differential equations. *Numerical Linear Algebra with Applications*, 27:e2286, 2020.
- [11] B. Beckermann, A.B.J. Kuijlaars. Superlinear convergence of conjugate gradients. *SIAM Journal on Numerical Analysis*, 39:300–329, 2001.
- [12] B. Beckermann, S. Serra-Capizzano. On the asymptotic spectrum of finite element matrix sequences. *SIAM Journal on Numerical Analysis*, 45:746–769, 2007.
- [13] P. Benedusi, P. Ferrari, M.E. Rognes, S. Serra-Capizzano. Modeling excitable cells with the EMI equations: spectral analysis and iterative solution strategy. *Journal of Scientific Computing*, 98(3):paper58, 23 pp., 2024.
- [14] M. Benzi, A. Frommer, R. Nabben, D.B. Szyld. Algebraic theory of multiplicative Schwarz methods. *Numerische Mathematik*, 89:605–639, 2001.
- [15] D. Bianchi, S. Serra-Capizzano. Spectral analysis of finite-dimensional approximations of 1D waves in non-uniform grids. *Calcolo*, 55:paper47, 2018.
- [16] D. Bianchi. Analysis of the spectral symbol associated to discretization schemes of linear self-adjoint differential operators. *Calcolo*, 58:paper38, 2021.

- [17] R. Bhatia. *Matrix analysis*. vol. 169 of Graduate Texts in Mathematics, Springer-Verlag, New York, 1997.
- [18] A. Böttcher, S.M. Grudsky. *Toeplitz Matrices, Asymptotic Linear Algebra, and Functional Analysis*. Birkhäuser Verlag, Basel, 2000.
- [19] A. Buffa, H. Harbrecht, A. Kunoth, G. Sangalli. BPX-preconditioning for isogeometric analysis. *Computer Methods in Applied Mechanics and Engineering*, 305:231–244, 2017.
- [20] X.-C. Cai, M. Sarkis. A restricted additive Schwarz preconditioner for general sparse systems. *SIAM Journal on Scientific Computing*, 21(2):792–797, 1999.
- [21] N. Collier, L. Dalcin, D. Pardo, V. Calo. The cost of continuity: performance of iterative solvers on isogeometric finite elements. *SIAM Journal on Scientific Computing*, 35(2):A767–A784, 2013.
- [22] M. Donatelli, C. Garoni, C. Manni, S. Serra-Capizzano, H. Speleers. Symbol-Based Multigrid Methods for Galerkin B-Spline Isogeometric Analysis. *SIAM Journal on Numerical Analysis*, 55(1):31–62, 2017.
- [23] A. Dorostkar, M. Neytcheva, S. Serra-Capizzano. Spectral analysis of coupled PDEs and of their Schur complements via generalized locally Toeplitz sequences in 2D. *Computer Methods in Applied Mechanics and Engineering*, 309:74–105, 2016.
- [24] M. Dumbser, F. Fambri, I. Furci, M. Mazza, S. Serra-Capizzano, M. Tavelli. Staggered discontinuous Galerkin methods for the incompressible Navier-Stokes equations: spectral analysis and computational results. *Numerical Linear Algebra with Applications*, 25(5):e2151, 2018.
- [25] E. Efstathiou, M.J. Gander. Why restricted additive Schwarz converges faster than additive Schwarz. *BIT Numerical Mathematics*, 43(5):945–959, 2003.
- [26] A. Frommer, D.B. Szyld. Weighted max norms, splittings, and overlapping additive Schwarz iterations. *Numerische Mathematik*, 83:259–278, 1999.
- [27] A. Frommer, D.B. Szyld. An algebraic convergence theory for restricted additive Schwarz Methods using weighted max norms. *SIAM Journal on Numerical Analysis*, 39(2):463–479, 2001.
- [28] M.J. Gander, S. Loisel, D.B. Szyld. An optimal block iterative method and preconditioner for banded matrices. *SIAM Journal on Matrix Analysis and Applications*, 33(2):653–680, 2012.
- [29] C. Garoni. Introduction to the theory of generalized locally Toeplitz sequences and its applications. *Mathematical Notes (in press); arXiv:2506.02151*, 2025.
- [30] C. Garoni, S. Serra-Capizzano. *Generalized locally Toeplitz sequences: theory and applications. Volume 1*. Springer, Cham, 2017. DOI: 10.1007/978-3-319-53679-8.
- [31] C. Garoni, S. Serra-Capizzano. *Generalized locally Toeplitz sequences: theory and applications. Volume 2*. Springer, Cham, 2018. DOI: 10.1007/978-3-030-02233-4.
- [32] C. Garoni, S. Serra-Capizzano. *Generalized locally Toeplitz sequences: a spectral analysis tool for discretized differential equations*. Splines and PDEs: from approximation theory to numerical linear algebra, 161–236, Lecture Notes in Mathematics, 2219, Fondazione CIME / CIME Foundation Subseries, Springer, Cham, 2018.
- [33] C. Garoni, S. Serra-Capizzano. Multilevel generalized locally Toeplitz sequences: an overview. *AIP Conference Proceedings*, 2116:020003, 2019.
- [34] C. Garoni, S. Serra-Capizzano. *Block Jacobi/Gauss–Seidel preconditioning for GLT sequences, and GLH sequences*. Submitted, 2025.
- [35] C. Garoni, S. Serra-Capizzano, D. Sesana. *Spectral analysis and spectral symbol of d-variate  $Q_p$  Lagrangian FEM stiffness matrices*. *SIAM Journal on Matrix Analysis and Applications*, 36(3):1100–1128, 2015.
- [36] C. Garoni, H. Speleers, S-E. Ekström, A. Reali, S. Serra-Capizzano, and T. J. R. Hughes. Symbol-based analysis of finite element and isogeometric B-spline discretizations of eigenvalue problems: exposition and review. *Archives of Computational Methods in Engineering*, 26(5):1639–1690, 2019, DOI 10.1007/s11831-018-9295-y.
- [37] G. H. Golub, C. F. Van Loan. *Matrix Computations, 4th edition*. Johns Hopkins University Press, Baltimore, 2013.

- [38] M. Griebel, P. Oswald. On the abstract theory of additive and multiplicative Schwarz algorithms. *Numerische Mathematik*, 70:163–180, 1995.
- [39] N.J. Higham. *Functions of Matrices: Theory and Computation*. SIAM, Philadelphia, 2008.
- [40] C. Hofreither, S. Takacs. Robust multigrid for isogeometric analysis based on stable splittings of spline spaces. *SIAM Journal on Numerical Analysis*, 55(4):2004–2024, 2017.
- [41] T.J.R. Hughes, J.A. Cottrell, Y. Bazilevs. Isogeometric analysis: CAD, finite elements, NURBS, exact geometry and mesh refinement. *Computer Methods in Applied Mechanics and Engineering*, 194:4135–4195, 2005.
- [42] A.B.J. Kuijlaars. Convergence analysis of Krylov subspace iterations with methods from potential theory. *SIAM Review*, 48: 3—40, 2006.
- [43] L. Laayouni, A. Ratnani, A. Rifqui. Optimized Schwarz Methods for Isogeometric Analysis. In *Domain Decomposition Methods in Science and Engineering XXVII*, pp. 335–342, Springer Nature Switzerland, Cham, 2024.
- [44] T. Mathew. *Domain Decomposition Methods for the Numerical Solution of Partial Differential Equations*. Lecture Notes in Computational Science and Engineering, 61, 2008.
- [45] R. Nabben, D.B. Szyld, Convergence Theory of Restricted Multiplicative Schwarz Methods. *SIAM Journal on Numerical Analysis*, 40(6):2318–2336, 2002.
- [46] A. Quarteroni, A. Valli. *Domain Decomposition Methods*. Clarendon Press, Oxford, 1999.
- [47] R. Rahla, S. Serra-Capizzano, C. Tablino-Possio. Spectral analysis of  $P_k$  finite element matrices in the case of Friedrichs-Keller triangulations via generalized locally Toeplitz technology. *Numerical Linear Algebra with Applications*, 27(4):e2302, 2020.
- [48] G. Sangalli, M. Tani. Isogeometric Preconditioners Based on Fast Solvers for the Sylvester Equation. *SIAM Journal on Scientific Computing*, 38:A3644–A3671, 2016.
- [49] S. Serra-Capizzano. Distribution results on the algebra generated by Toeplitz sequences: a finite-dimensional approach. *Linear Algebra and its Applications*, 328(1-3):121—130, 2001.
- [50] S. Serra-Capizzano. Generalized locally Toeplitz sequences: spectral analysis and applications to discretized partial differential equations. *Linear Algebra and its Applications*, 366:371–402, 2003.
- [51] S. Serra-Capizzano. The GLT class as generalized Fourier analysis and applications. *Linear Algebra and its Applications*, 419:180–233, 2006.
- [52] S. Serra-Capizzano. Spectral theory of matrix-sequences: perspectives of the GLT analysis and beyond. Proceedings of Numerical Analysis and Applications to Data Science-N2ADS 2025, Springer Proceedings on Mathematics and Statistics, in press.
- [53] B.F. Smith, P.E. Bjorstad, W.D. Gropp. *Domain Decomposition: Parallel Multilevel Methods for Elliptic Partial Differential Equations*. Cambridge University Press, Cambridge, UK, 1996.
- [54] W.P. Tang. Generalized Schwarz splittings. *SIAM Journal on Scientific and Statistical Computing*, 13(2):573–595, 1992.
- [55] A. Toselli, O. Widlund. *Domain Decomposition Methods – Algorithms and Theory*. Springer Series in Computational Mathematics, 34, 2005.